Iodide and chloride ions diffusivity, pore characterization and microstructures of concrete incorporating ground granulated blast furnace

(article starts on next page)

Original Article

Iodide and chloride ions diffusivity, pore characterization and microstructures of concrete incorporating ground granulated blast furnace slag

Hesong Jin [a], Zhenlin Li [a], Weizhuo Zhang [a], Jun Liu [a,b,*], Renbin Xie [a], Luping Tang [c], Jihua Zhu [a,b]

[a] College of Civil and Transportation Engineering, Shenzhen University, Shenzhen, 518060, PR China
[b] Guangdong Provincial Key Laboratory of Durability for Marine Civil Engineering, Shenzhen University, Shenzhen, 518060, PR China
[c] Department of Architecture and Civil Engineering, Division of Building Technology, Chalmers University of Technology, 41296, Gothenburg, Sweden

ARTICLE INFO

ABSTRACT

Innovative approaches are under research to study the resistance of chloride ion penetration in concrete containing chloride ions, to minimize the impact of chloride ion penetration test errors in coastal reinforced concrete (RC), which is helpful to the design of coastal RC structures. In this study, the diffusion depth, free ion concentration and diffusion coefficient of chloride, iodide ions with different curing ages and GGBFS content were measured by the Rapid Chloride Migration Test (RCM) and Rapid Iodide Migration tests (RIM). The SEM-EDS and MIP were used to analyze the microstructures, pore size distribution and the hydrated products. The results show that the performance of GGBFS concrete against the diffusion of corrosive ions is affected by the curing age and the content of GGBFS. With the increase of GGBFS content, especially concrete with 60% GGBFS, the influence of chloride, iodide ion penetrating into concrete gradually becomes smaller. The long-age curing system is more conducive to the concrete resistance to the migration and diffusion of chloride, iodine ions. Compared with the ordinary concrete, the total porosity of concrete mixed with GGBFS is lower, the internal microstructures have fewer cracks and defects, the density is better, and the diffusion coefficient of chloride and iodide ions is also lower. In addition, using the concept of corrosive ion adjustment coefficient (conversion coefficient of diffusion between chloride ion and iodide ion) and applying the data regression analysis (DRA), it is found that there is a good quadratic parabolic function relationship between the GGBFS content and the ions adjustment coefficient.

---

* Corresponding author.
E-mail address: liujun@szu.edu.cn (J. Liu).

1. Introduction

If reinforced concrete (RC) is exposed to harsh environments for a long time (such as marine environment, icy salt-except environment, etc.), its mechanical properties, durability, etc. will often be severely degraded. Among them, the corrosion of rebars is the most serious, which is mainly due to the corrosion of chloride ions inside the concrete, and when the chloride ion concentration reaches a critical threshold, the alkaline passivation film on the surface of the rebars is destroyed, causing corrosion of the rebars in the concrete [1—4]. This phenomenon is very common in coastal areas, and the comprehensive performance degradation of RC structures in this environment is very serious, especially the corrosion failure of rebars [5,6]. This will also result in other durability problems of the RC structures, such as cracking and falling off of the concrete cover layer, which seriously affects the service life of the RC structures and causes some waste of resources and economy [7,8]. In response to this problem, many scholars have conducted a lot of explorations on the mechanism of chloride ion transporting in concrete [9—13]. Among them, part of the researches on chloride erosion is carried out through salt leaching tests [14—18]. And the test results basically conform to Fick's II law or its modified equation. There is also a part of researches that simulates the atmospheric salt environment through salt spray tests. Studies have found that when RC is affected by atmospheric chlorides in coastal areas, the test results are likely to deviate from Fick's II law or its modified equation [19,20]. It should also be noted that because there are often some chloride ions inside the concrete, there are often certain errors in the test results obtained during the salt immersion test [21]. In addition, in coastal areas, RC structures are saturated with seawater for a long time, and are often affected by the alternation of high and low temperatures. At this time, the migration mechanism of chloride in the marine environment is more complicated [20]. Although some scholars have proposed that the diffusion mechanism of ions in concrete can be obtained by studying the penetration of iodide ions [21], there are still relatively few studies on the diffusion of iodide ions in concrete. Based on the above research backgrounds, to better understand the durability of concrete in the marine environment, it is of great significance to study the migration of chloride ions and iodide ions in concrete.

In recent decades, pozzolan materials (by-products or combustion residues of coal-fired power plants) are often used as the mineral admixtures in concrete, which can replace parts of ordinary Portland cement (OPC), which can save natural resources and contribute to environmental protection [22,23]. Among them, fly ash (FA) and ground granulated blast furnace slag (GGBFS) are the most common pozzolan materials. GGBFS is a commonly used active mineral admixture in concrete. The main chemical components of GGBFS are SiO_2, CaO, Al_2O_3 and MgO, in addition to FeO and a small amount of alkali. GGBFS is a glass body of the $CaO—SiO_2—Al_2O_3$ system. Its glass body content is high, the chemical structure is in a high-energy state, and its instability and potential activity are very large. The incorporation of GGBFS can reduce OPC hydration heat, improve impermeability and mechanical

strength and many other advantages, so it is widely used in actual RC structures [24—27].

Nowadays, concrete composed of OPC, silica fume, fly ash and GGBFS has gradually attracted the attention of civil engineering builders and scientific researchers, and some scholars have conducted some researches and analysis [23,28]. Research and exploration found that, obviously, these concretes with mineral admixtures have very good comprehensive properties (workability, mechanical properties, durability, ecological performance, economic performance, etc.), and they are also in line with the ideal requirements of RC structural design. Some scholars have recently conducted laboratory experiments to prove that concrete mixed with mineral admixtures has better durability [28,29]. Naturally, the attention of scientific researchers has gradually turned to the application of industrial by-product materials containing volcanic ash in concrete. And these mineral admixtures (fly ash, silica fume or GGBFS, etc.) have very important effects on the microscopic morphology, pore structures, mechanical properties, workability, and durability of concrete. The use of materials such as fly ash, silica fume or GGBFS has been shown to significantly affect the chemical properties of the pore distribution in the concrete matrix, thereby affecting the electrical conductivity of the concrete. Therefore, the addition of these mineral admixtures helps to ensure the operating life of the RC structure embedded with rebars [30—32]. The beneficial effects of GGBFS on RC have been recorded a lot, especially in corrosive environments rich in chloride and/or sulfate, such as coastal areas, offshore buildings, salt areas, and deicing salt highway environments. GGBFS thus adding to the concrete has been regarded as an effective means for the production of high-performance concrete [33,34]. Dhir et al. [35] studied the chloride binding capacity of the slurry under different GGBFS content and concluded: with the increase of the amount of GGBFS, the chloride binding capacity of the mixtures gradually increase, and the content of free chloride ions in the concrete gradually decreases. It is also found that the chloride ion binding capacity of cement pastes with the GGBFS content of 66.7% is about 5 times that of OPC pastes. Some studies believe that this ability is attributed to the formation of Friedel's salt inside the matrix [35,36]. In recent years, many scholars have conducted a lot of exploration and analysis on the durability of GGBFS concrete in coastal areas, but the understanding of the influence mechanism of chloride penetration in GGBFS concrete and the microstructures after chloride intrusion into GGBFS concrete is not very clear. Therefore, a comprehensive understanding of the ion transmission and diffusion mechanism of GGBFS concrete in the marine environment is of great significance, and it can provide some experience and reference for the later life design of GGBFS RC structures in coastal areas.

This study conducts RIM and RCM tests on GGBFS concrete of different curing ages and different GGBFS dosages, and mainly studies the influence of GGBFS on the penetration depth of iodide and chloride ions, and the concentration distribution of free iodide and chloride ions. Through MIP and SEM experiments, the effects of iodide and chloride ions on the pore structure and microscopic morphology of GGBFS concrete were analyzed. Finally, through data regression analysis, the correlation between the iodide ion and chloride

Table 1 − Chemical composition of OPC (%).

Materials	SiO$_2$	Al$_2$O$_3$	Fe$_2$O$_3$	CaO	MgO	SO$_3$	Na$_2$Oeq	f-CaO	Loss
Cement	22.87	4.47	3.48	64.05	2.46	2.44	0.52	0.9	1.21
GGBFS	34.33	13.60	14.89	26.87	8.15	0.23	−	−	1.93

ion diffusion coefficient of GGBFS concrete was studied, and the correlation equation was obtained. The effects of curing age and GGBFS content on the migration and microstructure of chloride ions are evaluated as a whole, and the feasibility of using iodide ions instead of chloride ions for the exploration of concrete ion diffusion performance when adding chloride ions inside the concrete is analyzed.

2. Raw materials and experimental program

2.1. Materials

The OPC used in this research project requires Portland cement without mineral admixtures. The P·I 42.5 benchmark cement produced by Shandong Lucheng Cement Co., Ltd. was used for concrete admixture inspection, conforming to Chinese standard GB175-2007 [63], and according to the ASTM C150 standard, the OPC can be about classified as Type I [37]. and the chemical composition, mineral composition and physical properties of OPC are shown in Table 1, Table 2, and Table 3. This test uses the S95 grade GGBFS produced by China's Jieyang Yongtai Slag Powder Factory, with a specific surface area of about 513 m^2/kg and according to the ASTM C989 standard it can be approximately classified as Grade 100 [64]. The chemical composition and performance indicators of GGBFS are shown in Tables 1 and 4. Other raw materials: (1). The river sand is as the fine aggregate, with a fineness modulus of 2.56 and an apparent density of 2635 kg/m^3, which meets ASTM C33/C33M [38]. (2). Graded gravel with a coarse aggregate particle size of 5 mm−25 mm, and this also meet the requirement of ASTM C33/C33M [38]. (3) Tap water is used for pouring and curing of specimens. (4) The configuration of the test solution uses deionized water. (5). The main chemicals include analytical pure NaCl, analytical pure NaI, analytical pure NaOH, analytical pure KIO$_3$, analytical pure AgNO$_3$, pure acetic acid and pure starch. The detailed description of the project was also published elsewhere [39].

2.1.1. Test plans
In the experiment, the proportions of GGBFS to replace the equivalent amount of OPC are 15%, 30%, and 60%, respectively and the curing age is 28 d and 150 d, respectively. Before the test, the test pieces need to be vacuum-saturated to make the inside of the concrete saturated, and then the RIM and RCM tests are carried out in the same environment. The test plan is shown in Table 5.

Table 2 − Mineral composition of OPC clinker (%).

C$_2$S	C$_3$S	C$_3$A	C$_4$AF
56.64	20.87	6.22	10.31

2.2. Determination of chloride and iodide ions diffusion coefficient

2.2.1. Rapid chloride ions migration coefficient method (RCM method)
The rapid electromigration chloride ion diffusion coefficient measurement method is also called the unsteady state rapid electromigration test method [21,65]: the test piece is placed between two electrolyte solutions and an external electric field is applied. The chloride ion in the cathode solution is tested under the action of the external electric field. Internal migration of files and the anolyte is 0.3 mol/L NaOH solution, and the catholyte is 10% NaCl solution. The RCM method is to test the chloride ion diffusion coefficient of concrete. Fig.1 is a schematic diagram of the RCM and RIM experimental devices. This test applied the NJ-RCM concrete chloride ion diffusion coefficient tester produced by Beijing Durable Weiye Company.

According to the NT-Build 443 and the method standard of GB/T 50082-2009 [39,40,41], the main steps of the RCM test are as follows: (1) The test pieces have a diameter of 100 mm ± 1 mm and a height of 50 mm ± 2 mm. And with a fine rasp, the permeating water sandpaper polished smooth surface. (2) Placing the test piece in a vacuum saturated water machine, then add saturated Ca(OH)$_2$ solution, dry pumping for 3 h, wet pumping for 1 h, and stopping for (18 ± 2) h. (3) The anolyte in the test is a 0.3 mol/L NaOH solution, and the catholyte is a NaCl solution with a mass fraction of 10%. (4) Recording the initial temperature, specimen height, energization duration, and targeting voltage of each channel, and recording the end temperature of each channel. (5) Splitting the test pieces along the axial direction on the compressive testing machine, and immediately spraying a 0.1 mol/L AgNO$_3$ solution on the section as a color indicator. (6) According to the obvious discoloration contour, measuring the penetration depth with a micrometer, and the result is accurate to 0.1 mm.

2.2.2. Rapid iodide ion diffusion method (RIM method)
The rapid electromigration iodide ion diffusion coefficient measurement method is also called the unsteady state rapid electromigration test method [21,65,66]: the test piece is placed between two electrolyte solutions and an external electric field is applied. The chloride ions in the cathode solution are tested under the action of the external electric field. Internal migration of files. The catholyte is 22.18% NaI solution, and the anolyte is 0.3 mol/L NaOH solution. The test method of the rapid iodide ion diffusion method (RIM) is very similar to the method of GB/T 50082-2009 and NT (NORDTEST) Build 443 [40,41], the test method and steps are roughly the same as the RCM method. The test equipment is shown in Fig. 1(b), and the main steps of the RIM test are as follows: (1) Testing solution: the catholyte is 22.18% NaI solution, the anolyte is 0.3 mol/L NaOH solution. (2) After the test pieces are

Table 3 – Physical properties of OPC.

Fineness	Density (g/cm^3)	Specific surface area m^2/kg	Standard consistency%	Stability mine method/mm	Setting time (min)		Flexural strength (MPa)		Compressive strength (MPa)	
					Initial setting	Final setting	3d	28d	3d	28d
0.8	3.15	341	25.8	0.2	142	207	5.7	–	26.2	–

Table 4 – Performance indicators of GGBFS (%).

Materials	Fineness (45 μm square hole sieve residue)	Water demand ratio	Loss on ignition	Water content	28 d compressive strength ratio
GGBF Slag	1.6	95.8	2.82	0.48	92.3

split, spraying 50% acetic acid solution on the surface immediately, and waiting for about 3 min. (3) Spraying a small amount of 10% potassium iodate solution and waiting for about 3 min. (4) Spraying a small amount of 5% starch suspension. After about 3 min, the penetration depth is measured to the nearest 0.1 mm.

2.2.3. Color development mechanism

(1) RCM test color development mechanism

The section of the concrete specimen is sprayed with 0.1 mol/L AgNO$_3$ solution, and there will be white precipitation in the chloride ion penetration area, which is mainly due to the chemical reaction Ag$^+$+Cl$^-$=AgCl. In the area outside the penetration of chloride ions, the OH$^-$ and Ag$^+$ in the cement paste react to form a brown Ag$_2$O precipitate, two different colors will form an obvious dividing line, and the penetration depth of chloride ions is measured by measuring the white precipitation area (Fig. 2(a)).

(2) RIM test color development mechanism

Starch is a white powder formed by polymerization of glucose molecules, composed of amylose (10%–30%) and amylopectin (70%–90%). Among them, amylose is soluble in water and has the characteristic of turning blue when exposed to iodine. Since iodine molecules will be decomposed into iodate and iodide in an alkaline environment (PH > 9), there is almost no iodine molecule (I$_2$+2OH$^-$→IO$^-$ + I$^-$ + H$_2$O). The color reaction of starch and iodine is the most sensitive in a weak acid environment of PH = 3–5. The concrete matrix is in a high-alkali environment, so first spraying acetic acid to acidify the surface of the specimen, and then spraying

potassium iodate to oxidize iodine ions into iodine molecules (5I$^-$ + IO$_3^-$+6H$^+$→3I$_2$+3H$_2$O) (Fig. 2(b)).

2.2.4. Calculation method of iodide ion and chloride ion diffusion coefficient

Obtaining the penetration depth of iodide and chloride ions, recording the relevant data during the test, calculating the iodide ion diffusion coefficient and chloride ion diffusion coefficient of concrete according to Eq. (1).

$$D = \frac{0.0239 \times (273 + T)L}{(U - 2)t}\left(X_d - 0.0238\sqrt{\frac{(273 + T)LX_d}{U - 2}}\right) \quad (1)$$

D——The non-steady ion diffusion coefficient of concrete, accurate to 0.1×10^{-12} m^2/s. **U** ——The absolute value of the voltage used (V). **T** ——The average value of the initial temperature and the end temperature of the anode solution (°C). **L** ——The thickness of the test piece (mm), accurate to 0.1 mm. **X$_d$** ——The average value of ion penetration depth (mm), accurate to 0.1 mm. **t** ——Test duration (h).

2.3. Determination of free iodide ion and chloride ion content

2.3.1. Powder sample preparation

After the RIM and RCM tests are over, using a mill to grind the concrete specimens in layers (shown in Fig. 3). Milling rule: starting from the ion penetration surface, according to the average penetration depth of the ions of the concrete specimens with different mix ratios, a sample is taken every 2 mm of grinding. The ground sample powders are passed through a 0.60 sieve, and then the powders are placed in a drying oven (60 ± 5) °C to dry to constant weight, the purpose is to remove the trace ions doped by the moisture in the powders [20].

2.3.2. Preparation of titration solution

The test method was carried out in accordance with the AASHTO T 260-97 2009 for water-soluble chloride ion content test [39,42]. The concrete powders after layered grinding is prepared into titration solution, and the content of free iodide and chloride ions in the concrete samples is determined by using automatic potentiometric titrator. The main steps are as follows, (1) Weighing 3 g of sample powder into a beaker, and drying it in an oven at 65 °C for 24 h (2) Then adding 60 ml–70 ml of deionized water and covering the glass dish. Using an

Table 5 – Corrosion ion diffusion test scheme of GGBFS concrete.

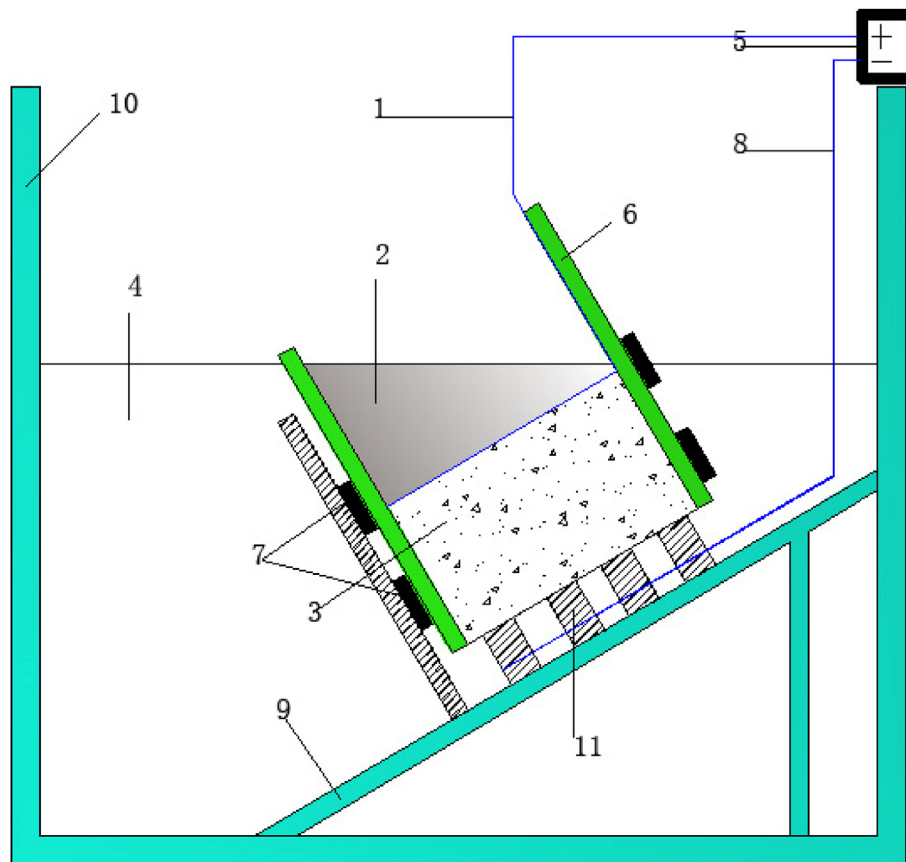| Dosage Curing age	S0	S15	S30	S60
28 d	RCM	RCM	RCM	RCM
	RIM	RIM	RIM	RIM
150 d	RCM	RCM	RCM	RCM
	RIM	RIM	RIM	RIM

Fig. 1 – RIM and RCM test. 1-anode plate; 2-anolyte; 3-concrete specimen; 4-catholyte; 5-DC stabilized power supply; 6- Rubber bucket; 7-hoop; 8-cathode plate; 9-support; 10-test tank; 11-support head.

electromagnetic stirrer to stir, heating the computer plate heating table to boiling for 5 min, and let it stand for 24 h (3) Using a double-layer filter paper funnel to filter the supernatant into a beaker, adding methyl orange indicator to the filtered solution, and dropping concentrated nitric acid until the solution turns red. (4) Finally, adding about 3 ml of 30% H_2O_2 solution to remove the sulfide in the samples. And making up the solution to 150 ml with deionized water.

2.3.3. Automatic potentiometric titration

This experiment uses the 809 Titrando automatic potentiometric titrator produced by Metrohm Company to measure the content of chloride and iodide ions.

The experiment uses 0.01 mol/L silver nitrate solution as the titrant. According to the volume of the consumed silver nitrate solution, the chloride ion content is calculated by Eq. (2), and the iodide ion content is calculated by Eq. (3).

$$Cl^-(\%) = \frac{3.5453 \times (V_1N_1 - V_2N_2)}{W} \quad (2)$$

$$I^-(\%) = \frac{12.6904 \times (V_1N_1 - V_2N_2)}{W} \quad (3)$$

In Eqs. (2) and (3), V_1 ——The volume of AgNO$_3$ solution consumed (ml). N_1——The concentration of AgNO$_3$ in the titrant (mol/L). W——the quality of the concrete sample
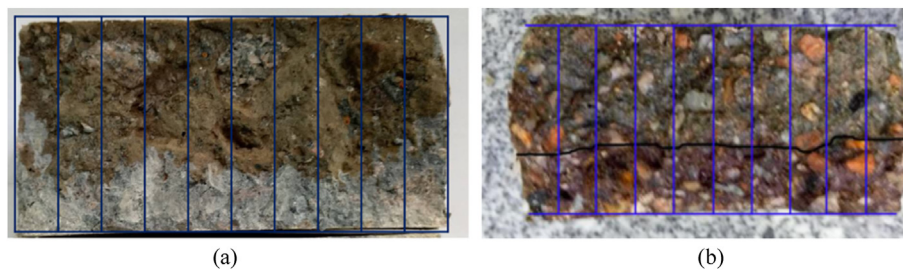

(a)   (b)

Fig. 2 – RCM color development and RIM color development. (a) RCM (b) RIM.
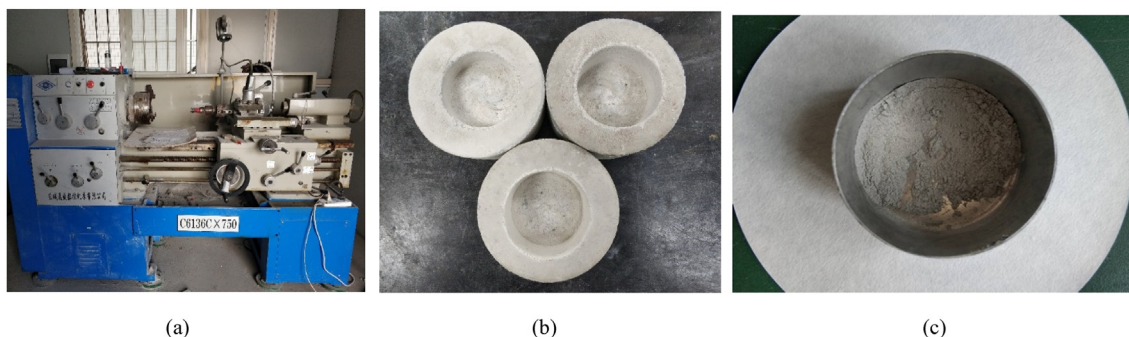
Fig. 3 — Grinding of GGBFS concrete specimens. (a) Pulverizer (b) Pulverized test pieces (c) Concrete powders.

powders. V_2——The volume of NaCl solution added (ml). N_2——The concentration of the added NaCl solution (mol/L).

2.4. Microstructure test

2.4.1. MIP
The conventional method for studying the pore structure of materials is MIP, and mercury intrusion instruments (Autopore IV 9500 porosimeter, Micromeritics, USA) are often used to test the pores of slurry mixtures. The samples used in this study are taken from the surface of concrete or mortar, the diameter of the test samples is approximately 10 mm—15 mm, and the samples are placed in an oven at 60 °C for 24 h before the test [43].

2.4.2. SEM-EDS
This study uses scanning electron microscopy-energy dispersive spectrum experiments (Its model is Quanta TM 250 FEG, manufactured by FEI Company, America) to analyze the microscopic morphology of concrete. SEM requires the test samples to be approximately 15 mm in diameter and 10 mm—15 mm in thickness. In this study, the mixtures on the surface of the specimens were cut and sampled. Because concrete has extremely poor electrical conductivity, the samples needed to be treated with gold plating before the experiment [43].

2.4.3. XRD
To explore the phase analysis of concrete, this study uses an X-ray diffractometer (its model is MICROXCT-400, which is manufactured by XRADIA, USA). In the experiment, the XRD scan angle was set within the 2θ range of $5°$—$80°$. The sample needs to be ground into very fine powder particles, which are taken from the inside of the concrete mortar, and the sand and gravel aggregates need to be removed. The powder particles need to be dried before the experiment [66].

3. Results and discussions

3.1. The influence of GGBFS on the penetration depth of iodide and chloride ions

The GGBFS concrete specimens with curing ages of 28 d and 150 d were subjected to RIM and RCM tests. The results of the penetration depth of iodide and chloride ions of the GGBFS concrete are shown in Fig. 4.

Sample 1, Sample 2, and Sample 3 in Fig. 4(a—d) represent three test pieces with the same mix ratio. It can be seen from Fig. 5(a) that the content of GGBFS is in the range of 0%—60%. As the content of GGBFS increases, the depth of chloride ion penetration in GGBFS concrete gradually decreases. Similarly, in Fig. 4(b), it can be seen that the penetration depth of concrete iodide ion is similar to chloride ion, and it decreases with the increase of GGBFS content. This shows that GGBFS better improves the ion permeability resistance of concrete. It can be seen from Fig. 4(c—d) that when the curing age is 150 d, the penetration depth of chloride ions and iodide ions of GGBFS concrete also decreases with the increase of GGBFS content. And at the same GGBFS volume, the iodine ion penetration depth of the 150 d specimens is smaller than that of the 28 d specimens. This is because with the longer the curing time, the more fully the OPC and GGBFS hydration is, the denser is the interior of the GGBFS concrete, and the stronger is its impermeability.

The incorporation of GGBFs greatly improves the anti-ionic permeability of concrete. It can be found from Fig. 4 (e), when the curing age is 28 days, GGBFs content ranges from 15% to 30%—60%, and the average penetration depth of chloride ions is 16.18 mm, 11.99 mm and 9.70 mm respectively, which decreases by 37.38%, 53.59% and 62.46% respectively compared with the specimen S0 without GGBFs. Similarly, the average penetration depths of iodide ions were 18.82 mm, 12.98 mm, and 10.28 mm, respectively, which were reduced by 31.35%, 54.34%, and 59.97% compared with the sample S0 without GGBFS. It can be seen that GGBFS has similar effects on the penetration depth of iodide and chloride ions in GGBFS concrete.

Comparing the average penetration depth of iodide ions and chloride ions in the 28-day specimens, the difference between the two values is 2.64 mm, 0.99 mm, and 0.58 mm, respectively. It can be seen that there is not much difference between the penetration depth of iodide ion and chloride ion. With the greater the content of GGBFS, the smaller the difference in penetration depth is. It can be found from Fig. 5(f) that when the curing age is 150 d, the average penetration depth of chloride ions of the specimens S15, S30, and S60 becomes 14.63 mm, 9.73 mm, 8.53 mm, respectively, which is reduced by 31.35%, 54.34%, and 59.97%, respectively, compared with the specimen S0 without adding GGBFS. The
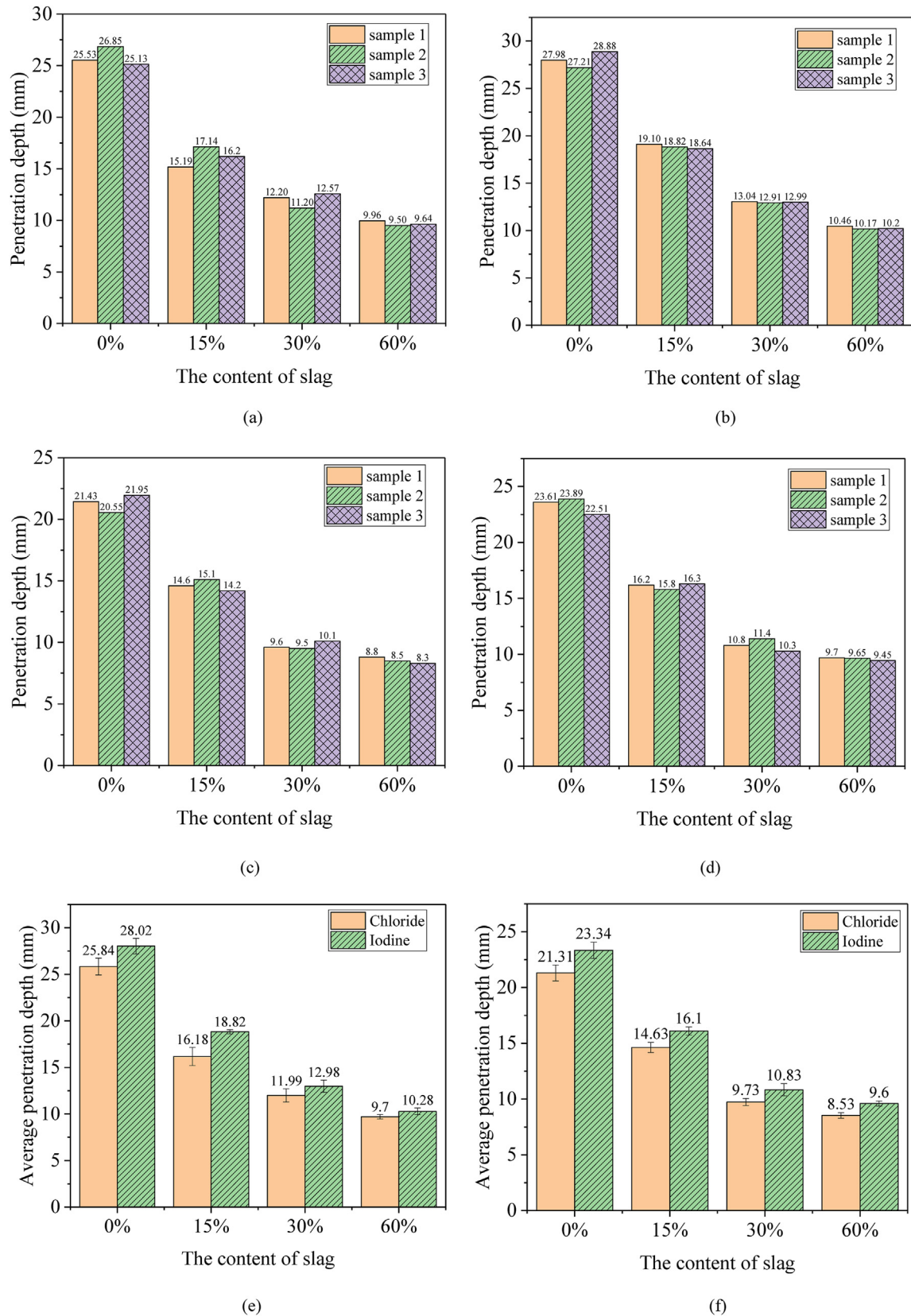
Fig. 4 − **Ion penetration depth of GGBFS concrete at different curing ages. (a) Chloride ion penetration depth of 28 d GGBFS concrete (b) Iodine ion penetration depth of 28 d GGBFS concrete, (c) Chloride ion penetration depth of 150 d GGBFS concrete (d) Iodine ion penetration depth of 150 d GGBFS concrete. (e) The average ion penetration depth of 28 d GGBFS concrete (f) The average ion penetration depth of 150 d GGBFS concrete.**
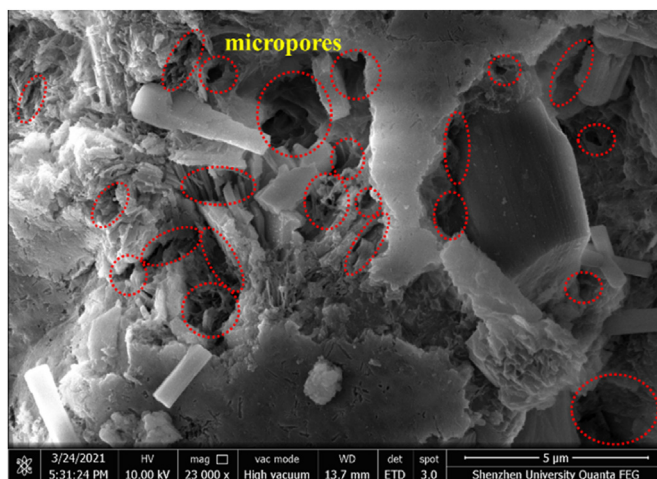
Fig. 5 — Micropores in concrete.

average penetration depth of iodide ions was 16.10 mm, 10.83 mm, and 9.60 mm, respectively, which decreased by 31.02%, 53.6%, and 58.87% respectively. Comparing the average penetration depth of iodide ions and chloride ions of 150-d specimens, the difference between the two values is 1.47 mm, 1.10 mm, 1.07 mm, and the results are not much different. It shows that the penetration depth of iodide ion and chloride ion in 150 d GGBFS concrete also has a good correlation. In addition, according to Fig. 4(e—f), as the curing age increases and the GGBF slag content increases, the diffusion depth difference between iodide ions and chloride ions gradually decreases, for example, from 2.2 mm for S0-28d to 0.3 for S0-28 d mm. This is mainly because when the concrete contains chloride ions, the chloride content measured by the RCM method is the sum of the external environment and the internal chloride, while the RIM method can only measure the concentration of iodide and is not affected by the chloride ions inside the concrete. Overall, the RIM method can better reflect the performance of chloride-containing concrete against the penetration and diffusion of chloride ions. This RIM method has been popularized and applied in our other literature [66]. Literature [66] studied the resistance of concrete components contaminated by deicing salt to corrosive ions. And the results show that it is very valuable to use RIM to test the environmental effect depth of chloride-containing concrete.

Overall, with the increase in the amount of GGBFS, the performance of GGBFS concrete to resist the diffusion of chloride and iodide ions gradually improves. As well known, because GGBFS can react with calcium hydroxide or alkali released during the hydration process of OPC, the utilization of GGBFS in concrete production can change the pore size of concrete and reduce the permeability of concrete. In addition, when some amount of GGBF slag is added to concrete, in the OPC system, GGBF slag, OPC and free water undergo hydration reaction, and there will be many gel compounds in the matrix, and the alkaline medium in these hydration products can stimulate GGBF slag further hydrates. Because the OPC system is an alkaline environment, the surface of these GGBF Slag glass bodies will be continuously destroyed by the OH^- in the OPC system. This also promotes further depolymerization of GGBF slag, and various ions after depolymerization will

diffuse and penetrate into the concrete with the pore solution. The OH^-, H^+, etc. in the pore solution of the cement matrix are adsorbed by the Ca^{2+} and Mg^{2+} on the surface of the GGBF slag, thereby forming a gel, and will promote the full hydration of the GGBF Slag glass body, which accelerates the hydration of the cementitious material in the concrete matrix. When the OH^-, Ca^{2+}, H_2O in the matrix react with the SiO_2 in the glass body of the GGBF Slag, the $CaO–SiO_2–H_2O$ (C–S–H) gel is formed. Therefore, when the content of GGBF slag is higher, the molar ratio of Ca/Si in the matrix is lower, which leads to good cementitious performance between C–S–H gels. This also significantly improves the microstructure of the concrete matrix, thereby increasing the compactness of the concrete. Similar conclusions have also been found in the literature [66]. Therefore, adding GGBFS can enhance the pore densification and connectivity of the concrete matrix [44], and the density of the GGBFS concrete matrix gradually increases. Therefore, compared with OPC concrete, the penetration depth of corrosive ions in GGBFS concrete is relatively small. This is consistent with the results of the literature [45—48]. Gesoglu et al. [45] studied the resistance to chloride ion permeability and water permeability of GGBFS, fly ash and silica fume self-compacting concrete. In that study, it was found that with the use of mineral admixtures, the permeability of chloride ions is getting better and better. The chloride ion permeability of 20%, 40% and 60% GGBFS concrete decreased from 2065 C to 1053 C, from 2065 C to 403 C and from 2065 C to 282 C, respectively. This is consistent with the research results of this study, and both show that adding GGBFS to concrete is a cheap and easy-to-solve effective solution to resist the diffusion of chloride ions in concrete. This is mainly because the macropores and capillary pores in the concrete matrix become gel pores and transition pores, and the pore diameter is less than 5 μm, this also can be found in Fig. 5, and the literature [46—48] also found these similar results. In addition, the long curing age system is more conducive to the resistance of GGBFS concrete to the diffusion of corrosive ions, which has also been confirmed in the literature [49]. Guneyisi and Gesoglu [49] also studied the comprehensive effects of curing methods and high substitution levels of GGBFS on the chloride ion permeability of high-performance

concrete. The study found that regardless of the curing conditions, the chloride ion diffusion effect of GGBFS concrete is significantly worse than that of concrete without GGBFS. And the concrete containing over 50% GGBFS, under all curing conditions and test ages, the value of charged chloride ion is significantly reduced, which is almost similar to the results of this study.

3.2. *GGBFS effect of free iodine and chloride ions concentration distribution*

It can be seen from Fig. 6(a) that the free iodide ion concentration in GGBFS concrete is significantly lower than that of ordinary concrete without GGBFS. With the increase of GGBFS content, the free iodide ion concentration in concrete gradually decreases. Among them, the concentration of free iodide ions drops sharply in the zone of penetration depth 0 mm−5 mm. The free iodide ion concentration of GGBFS specimens

S0, S15, S30 and S60 decreased by 0.52%, 0.46%, 0.37%, and 0.34%, respectively, and the proportion of the decrease was 41.32%, 42.60%, 42.70%, 59.21%, respectively. After the penetration depth is greater than 5 mm, the free iodide ion concentration gradually decreases. And as the penetration depth is greater than 5 mm, the content of corrosive ions in the concrete gradually decreases, and the corrosive ion content curve gradually becomes flat with the increase of penetration depth. Similar research phenomena have also been found in literature [8,20]. And when the penetration depth is the same, with the higher the content of GGBF Slag, the lower is the content of corrosive ions in the concrete. This also shows that GGBF Slag helps to improve the compactness of concrete and reduce the total porosity of concrete. Similar research results have also been found in the literature [66]. Similarly, it can be seen from Fig. 6(b) that as the content of GGBFS increases, the concentration of free chloride ions in concrete also gradually decreases, and the downward trend is similar to that of free
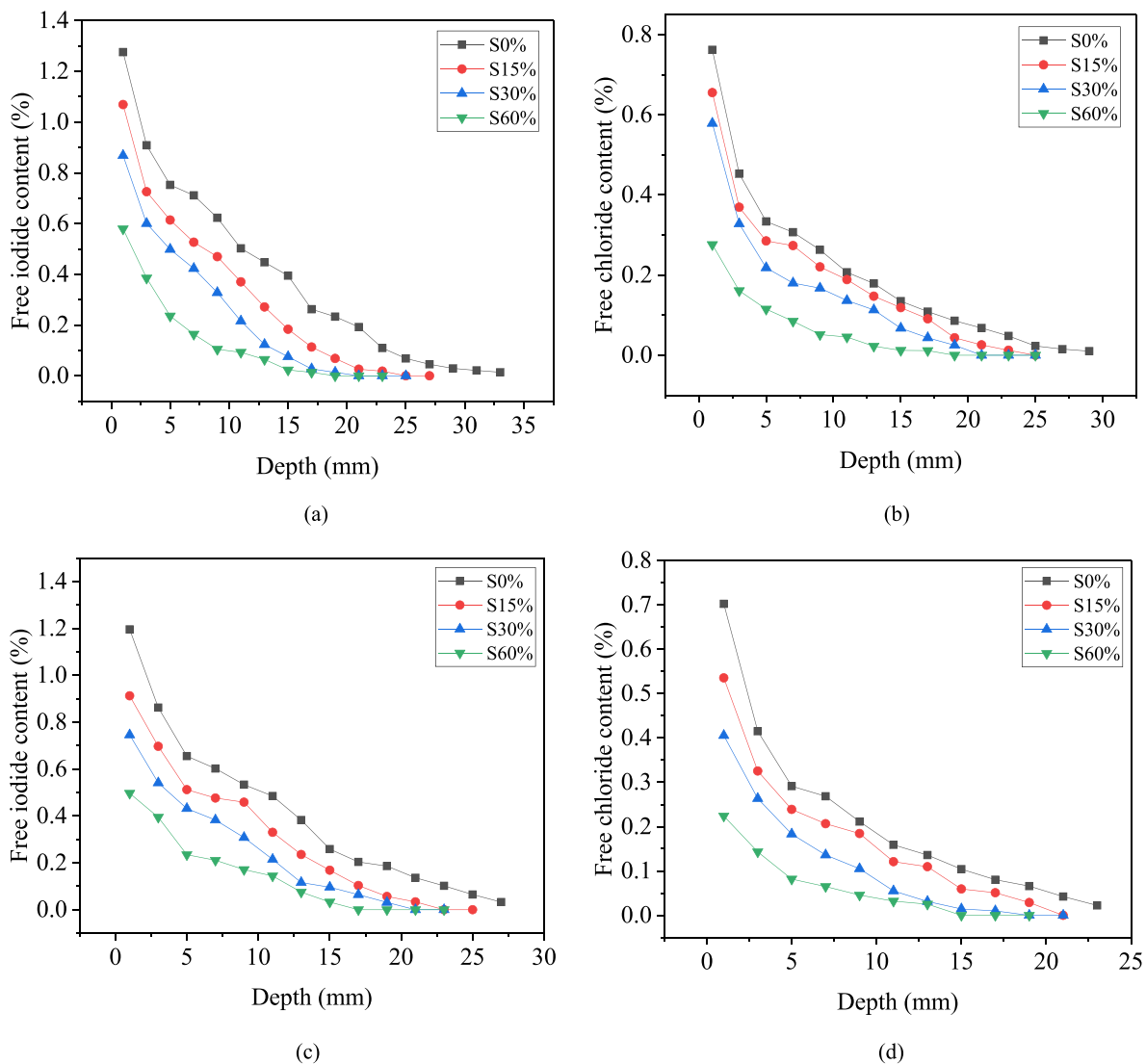

(a)

(b)

(c)

(d)

Fig. 6 − The distribution of ions in GGBFS concrete under different curing ages. (a) Concentration distribution of free iodide ion at28 d. (b) Concentration distribution of free chloride ion at 28 d. (c) Concentration distribution of free iodide ion at 150 d. (d) Concentration distribution of free chloride ion at 150 d.

iodide ions. Within the penetration depth of 0 mm—5 mm, the free chloride ion concentration of GGBFS specimens S0, S15, S30 and S60 decreased by 0.43%, 0.37%, 0.36% and 0.16%, respectively, and the decreasing proportions were 56.21%, 56.50%, 63.32% and 58.33%, respectively. From the above analysis, it can be concluded that for the 28-day GGBFS concrete, the free chloride ion concentration drops in the ranges of 56.21%—62.31%, and the free iodide ion drops in the range of 41.32%—59.21%. The above analysis shows that the GGBFS concrete with an age of 28 days has a good correlation between the free iodide ion and chloride ion concentration distribution.

When considering the age of 150 d, it can be found from the above figure that at the same penetration depth, the concentration of free chloride and iodide at 28 d is greater than the ion concentration at 150 d. This shows that with the longer the curing age, the better the impermeability of GGBFS concrete to iodide and chloride ions is. This is because OPC hydration is a continuous process for a long period of time. The C—S—H gel keeps increasing, the pores keep decreasing, and the pozzolanic effect of GGBFS gradually appears, which promotes cement hydration and makes the concrete interior become more and more dense. From Fig. 6(c—d), it can be found that within the penetration depth of 0—5 mm, the free iodide ion concentration of the specimens S0, S15, S30, and S60 decreased by 0.54%, 0.40%, 0.31%, 0.26%, respectively. The proportions of decline were 45.12%, 43.85%, 42.10%, and 52.80% respectively. The free chloride ion concentration of specimens S0, S15, S30, and S60 decreased by 0.41%, 0.29%, 0.22%, and 0.14%, respectively, and the proportion of the decrease was 58.51%, 55.30%, 54.82%, and 63.40%, respectively. Therefore, within 0 mm—5 mm of concrete, with the increase of GGBFS content, the decrease rate of iodide ion and chloride ion concentration in the concrete gradually decreases. The above analysis shows that the GGBFS concrete with the curing age of 150 days has a good linear correlation between the free iodide ion and chloride ion concentration distribution.

The incorporation of GGBFS improves the resistance of concrete to chloride ions and iodide ions. On the one hand, the filling effect of GGBFS powder makes the interior of the concrete more compact, reduces the porosity, and improves the resistance of GGBFS concrete to ion permeability. The external aspect is the physical adsorption and chemical combination of chloride ions by GGBFS. The secondary hydration reaction of GGBFS in the concrete produces more C—S—H gels, and more C—S—H gels can adsorb more iodide and chloride ions. In addition, some studies have shown that the compound gel and microscopic pores in the concrete matrix will affect the concrete's resistance to corrosive ion penetration and diffusion [67]. And when the content of GGBF Slag in the concrete is less than 50%, the chloride is more likely to be adsorbed in the C—S—H gels due to the effect of charge ion balance [68]. Therefore, the content of GGBF Slag is an important factor affecting the chloride content in concrete. Some studies have found that when the content of GGBF Slag is greater than 50%, the main hydration product in concrete is C-A-S-H gel [69,70]. The hydration reaction of this gel is different from the hydration reaction of C—S—H gel. C-A-S-H gel can combine free water to form crystals [66]. As a result, these compound

products can fill the pores of the matrix, change the curvature and quantity of the pores of the matrix, thereby improving the compactness of the concrete, which reduces the permeability of corrosive ions in the concrete. Therefore, it is not difficult to find in this study that when the content of GGBF Slag is higher, the content of corrosive ions in concrete is relatively low, which also shows that the content of GGBF Slag directly affects the ability of concrete to resist the migration of corrosive ions. Overall, this can be used as an effective method to improve the ability of concrete structures to resist corrosive ion migration, which is very similar to the research conclusions of literature [67].

In addition, GGBFS contains more Al_2O_3, and its hydrated product calcium aluminate hydrate reacts with chloride ions to form calcium chloroaluminate hydrate [50,51], which is commonly the Friedel salt ($C_3A \cdot CaCl_2 \cdot 10H_2O$). The iodide ion reacts with calcium chlorate hydrate to form calcium iodoaluminate hydrate [52], the chemical formula is shown in Eqs. (4) and (5), and the Compound products of iodide ion and chloride ion is $3CaO \cdot Al_2O_3 \cdot CaI_2 \cdot 8H_2O$ and $C_3ACaCl_2 \bullet 10H_2O$. The above effects all increase the ability of concrete to hinder iodine and chloride ions.

$$C_3A + CaCl_2 + 10H_2O \rightarrow C_3ACaCl_2 \bullet 10H_2O \tag{4}$$

$$C_3A + CaI_2 + 8H_2O \rightarrow C_3ACaI_2 \bullet 8H_2O \tag{5}$$
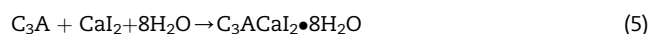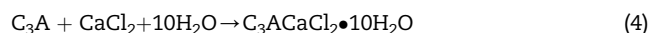
3.3. Correlation analysis of iodide ion and chloride ion diffusion coefficient of GGBFS concrete

3.3.1. The influence of GGBFS on the diffusion coefficient of iodide and chloride ions

Performing RCM and RIM tests on GGBFS concrete with different content at the same time, recording relevant data, measuring the average penetration depth of iodide and chloride ions, and then calculating the diffusion coefficient of iodide and chloride ions according to Eq. (1), the result is shown in Fig. 7. It can be clearly seen from Fig. 7 that as the content of GGBFS increases, the diffusion coefficients of iodide ions and chloride ions gradually decrease, and the diffusion coefficients of iodide ions are slightly larger than the diffusion coefficients of chloride ions.

The chloride ion diffusion coefficients of the 28-day specimens S0, S15, S30 and S60 are 11.95×10^{-12} m^2/s, 7.58×10^{-12} m^2/s, 3.97×10^{-12} m^2/s and 3.16×10^{-12} m^2/s respectively. The iodide ion diffusion coefficients are 12.97×10^{-12} $m^2/$, 8.62×10^{-12} m^2/s, 4.64×10^{-12} m^2/s and 3.65×10^{-12} m^2/s respectively. The proportions of iodide ion diffusion coefficient higher than chloride ion diffusion coefficient are 8.51%, 13.71%, 16.88%, 15.34%, respectively. In addition, it can be found that when the GGBFS content is greater than 30%, the reduction of the diffusion coefficients of iodide and chloride ions has been slowed down. It shows that the GGBFS content has a maximum effect on the improvement of concrete anti-ionic permeability. If this maximum value is exceeded, the improvement effect becomes less obvious.

The pozzolanic effect of GGBFS reduces the amount of hydrated $Ca(OH)_2$ in the coarse crystals of the concrete, and
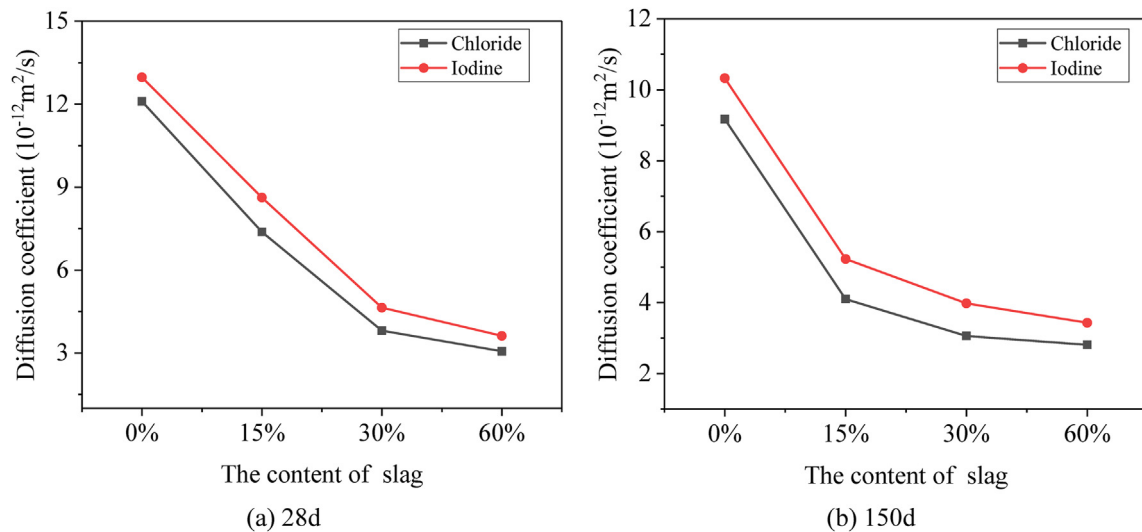
Fig. 7 − Comparison of iodide ion and chloride ion diffusion coefficients of GGBFS concrete at different curing ages.

promotes the hydration of the cement to produce more high-strength, stable and low-alkaline C−S−H gels, thereby improving the internal structure of the concrete compactness [44]. When the amount of GGBFS exceeds a certain amount, the insufficient amount of Ca(OH)$_2$ in the concrete affects the play of the pozzolanic effect of GGBFS, resulting in a slight decrease in the anti-ion penetration performance of the concrete. It can be seen from the above analysis that GGBFS has similar effects on concrete iodide ion diffusion coefficient and chloride ion diffusion coefficient, and they have a good correlation. And with the gradual increase of the curing age and the content of GGBFS, the diffusion coefficient of corrosive ions gradually decreases, which is consistent with the research conclusion of the literature [45].

3.3.2. Correlation of GGBFS concrete iodide ion and chloride ion diffusion coefficient

A large number of RC structures are inevitably corroded by chloride ions in the environment during service. The chloride ions inside the concrete will affect the accuracy of the chloride ion diffusion coefficient measured by the RCM, and the test results will be completely distorted. This study applies the iodide ion diffusion coefficient measured by the RIM to find out the correlation between the iodide ion and chloride ion diffusion coefficient, and uses it to evaluate the durability of concrete. From the analysis of the above section 3, it can be found that the iodine ion diffusion coefficient and chloride ion diffusion coefficient of GGBFS concrete have a good correlation, and under the same mix ratio, the iodine ion diffusion coefficient is slightly larger than the chloride ion diffusion coefficient. For the specimens with a curing age of 28 days, the iodide ion diffusion coefficient is 1.085−1.169 times of the chloride ion diffusion coefficient. For the specimens with a curing age of 150 days, the iodide ion diffusion coefficient is 1.119−1.184 times of the chloride ion diffusion coefficient.

To study the correlation between the iodide ion diffusion coefficient and chloride ion diffusion coefficient of concrete mixed with GGBFS at the curing age of 28 days, Data

regression analysis on GGBFS content x and adjustment coefficient "α" was conducted, which can be obtained by D (Cl$^-$) = "α" × D (I$^-$). The data regression analysis result is shown in Fig. 8,

$$\alpha = 0.9217 - 0.3468x + 0.4263x^2 \qquad (6)$$

According to Table 6, although the error values of the three specimens in the control group and the concrete group mixed with GGBF Slag are different. For example, the error values of S0-2 and S0-3 in the control group are very close, but significantly higher than S0-1, the error value of S60-1 is 0.92%, the error value of S60-2 is 0.27%, and the error value of S60-3 is 0.65%, but their error values are all less than 1%. This is mainly because the internal microstructure of each group of concrete is different, which leads to differences in the penetration and diffusion of corrosive ions, which can be verified in Section 3.4 and Section 3.5. But on the whole, the error between the
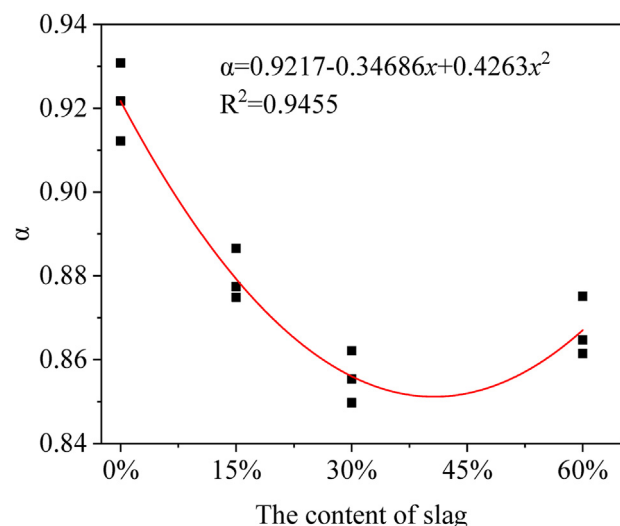

Fig. 8 − Fitting of GGBFS content and adjustment coefficient "α" at 28d curing age.

Table 6 — Comparison of iodide ion and chloride ion diffusion coefficient of GGBFS concrete under 28 d curing age.

Code	D (I⁻) × 10⁻¹² m²/s	Adjustment coefficient α	After conversion D (I⁻)	D (Cl⁻) × 10⁻¹² m²/s	Error value (positive value)
S0-1	12.78	0.921	11.78	11.78	0.03%
S0-2	13.15	0.921	12.12	12.24	0.98%
S0-3	12.98	0.921	11.96	11.84	1.04%
S15-1	8.11	0.879	7.13	7.19	0.82%
S15-2	8.76	0.879	7.71	7.69	0.21%
S15-3	8.98	0.879	7.90	7.86	0.50%
S30-1	4.42	0.856	3.78	3.81	0.71%
S30-2	4.65	0.856	3.98	3.98	0.07%
S30-3	4.85	0.856	4.15	4.12	0.74%
S60-1	3.57	0.867	3.09	3.12	0.92%
S60-2	3.69	0.867	3.20	3.19	0.27%
S60-3	3.69	0.867	3.20	3.18	0.65%

predicted value of concrete and the test value is basically less than 1%, which also shows that the predicted value and the error value are almost the same. Therefore, it can be considered that the RIM test method can replace the RCM method to predict the performance of the chloride-containing concrete against the migration of chloride ions. In addition , it can be seen from Table 6 that the iodide ion diffusion coefficient of GGBFS concrete obtained by RIM test. After adjusting the co-efficient "α" transformation, the obtained chloride ion diffusion coefficient is compared with the chloride ion diffusion coefficient measured by RCM, and the test error range is 0.03%—1.04%, which basically meets the engineering accuracy requirements. Therefore, the iodide ion diffusion coefficient of 28 d GGBFS concrete can be used as the chloride ion diffusion coefficient of GGBFS concrete after the corrosion ion adjustment coefficient is converted.

Similarly, to study the correlation between the iodide ion diffusion coefficient and chloride ion diffusion coefficient of 150-day concrete mixed with GGBFS, data regression analysis on GGBFS content **x** and adjustment coefficient β was conducted, which can be obtained by D (Cl⁻) = β × D (I⁻). The data regression analysis result is shown in Fig. 9,

$$\beta = 0.8937 - 0.1859x + 0.1723x^2 \tag{7}$$

According to Table 7, although the error values of the three specimens in the control group and the concrete group mixed with GGBF Slag are different. For example, the error value of S30-2 in the control group is 0.21%, the error value of S30-2 is 0.29%, but it is significantly higher than the 0.05% of S0-1, the error value of S0-1 is 0.46%, and the error value of S0-2 is 0.99%, S0-3 error value is 0.29%, but their error values are all less than 1%. This is mainly due to the different types of internal pores, porosity, and micro-combination products of each group of concrete, which leads to differences in the penetration and diffusion of corrosive ions in the concrete. This is in Section 3.4 and Section 3.5. All have been verified. But on the whole, the error between the predicted value and the test value of concrete is basically less than 1%, which also shows that the predicted value and error value of chloride in concrete are almost the same. Therefore, this also shows that the RIM test method can replace the RCM method to predict the performance of the chloride-containing concrete against the migration of chloride ions. Similarly, it can be seen from

Table 7 that the iodide ion diffusion coefficient of 150 d GGBFS concrete obtained by RIM test is transformed by the adjustment coefficient β, and the chloride ion diffusion coefficient obtained is compared with the chloride ion diffusion coefficient measured by RCM. The test error value range is 0.05%—1.34%, which basically meets the engineering accuracy requirements. Therefore, the iodide ion diffusion coefficient of GGBFS concrete under the curing age of 150 days can be used as the chloride ion diffusion coefficient of GGBFS concrete after being transformed.

Generally speaking, when the curing age is 28 days, GGBFS is in the early stage of hydration in concrete and cannot be fully hydrated. When the curing age is 150 days, GGBFS is in the late hydration stage of concrete, which is close to complete hydration [53]. To simplify Eqs. (6) and (7), within the curing age range of 28 d—150 d, Eq. (6) can be used to calculate the adjustment coefficient of GGBFS concrete. For GGBFS concrete with the curing age of more than 150 days, the adjustment coefficient can be calculated by Eq. (7), so Eq. (8) is the calculation formula for the corrosive ion adjustment co-efficient of GGBFS concrete under different curing ages.

$$\begin{cases} \alpha = 0.9217 - 0.3468x + 0.4263x^2 & Curing\ days < 150d \\ \beta = 0.8937 - 0.1859x + 0.1723x^2 & Curing\ days > 150d \end{cases} \tag{8}$$

$$\beta = 0.8937 - 0.1859x + 0.1723x^2$$
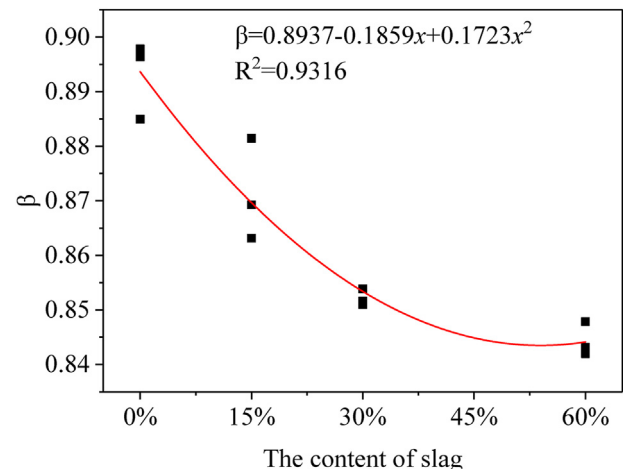$$R^2 = 0.9316$$

Fig. 9 — Fitting of GGBFS content and adjustment coefficient β under 150 d curing age.

Table 7 − Comparison of iodide ion and chloride ion diffusion coefficient of 150-d GGBFS concrete.

Number	$D\ (I^-) \times 10^{-12}\ m^2/s$	Adjustment coefficient α	After conversion $D\ (I^-)$	$D\ (Cl^-) \times 10^{-12}\ m^2/s$	Error value (positive value)
S0-1	9.88	0.893	8.83	8.87	0.46%
S0-2	10.77	0.893	9.62	9.53	0.99%
S0-3	10.16	0.893	9.08	9.11	0.29%
S15-1	5.01	0.869	4.36	4.42	1.34%
S15-2	4.99	0.869	4.34	4.34	0.05%
S15-3	5.06	0.869	4.40	4.37	0.76%
S30-1	3.83	0.853	3.27	3.26	0.21%
S30-2	3.78	0.853	3.23	3.22	0.29%
S30-3	3.88	0.853	3.31	3.31	0.05%
S60-1	3.45	0.844	2.91	2.91	0.12%
S60-2	3.37	0.844	2.85	2.86	0.43%
S60-3	3.33	0.844	2.82	2.81	0.26%

3.4. Pore structure analysis

The specimens with GGBFS content (0%, 15%, 30%, 60%) were subjected to RIM and RCM tests, and the pore structure of the specimens was tested according to the MIP introduced in Section 2. From the cumulative pore size distribution curves in Fig. 10(a−b), it can be seen that after iodide and chloride ions invade the specimens, the cumulative pore size distribution of the ordinary concrete S0 specimens is larger than the GGBFS concrete specimens. Cumulative pore size represents the total void volume of concrete measured by MIP, which shows that the incorporation of GGBFS reduces the pore volume of concrete. As the amount of GGBFS increases, the cumulative pore size gradually decreases.

In addition, in the differential pore size distribution of concrete, the peak of the curve indicates that the proportion of pores with the pore size is the largest, which is called the most probable pore. From the differential pore size distribution in Fig. 10(c−d), it can be seen that after the RIM test, the most probable pore of the specimen S0 is 81 nm, the most probable pore of the specimen S15 is 50 nm, the most probable pore of the specimen S30 is 32 nm, and the most probable pore of the specimen S60 is 26 nm. Similarly, after the RCM test, the most probable pore of specimen S0 is 77 nm, the most probable pore of specimen S15 is 53 nm, the most probable pore of specimen S30 is 28 nm, and the most probable pore of specimen S60 is 30 nm.

The increase of GGBFS content makes the peak on the differential distribution curve shift to the left side of the small pore direction. This is mainly because GGBFS promotes cement hydration, generates more and more abundant hydration products, fills the pores, and increases the number of gel pores. In addition, the solid phase product Friedel salt formed by the chemical combination of iodide and chloride ions with the cement phase will reduce the number of macropores and thereby reduce the porosity of the concrete paste [54]. By comparing the most probable pore of RCM and RIM specimens, it can be seen that iodide ions and chloride ions have similar effects on the most probable pore size of GGBFS concrete, and both decrease with the increase of GGBFS content. According to the previous literature [66,71], GGBF slag has pozzolanic effect, micro-aggregate effect and microcrystalline nucleus effect. Because GGBF slag has higher activity than fly ash, the addition of high content of GGBF slag in

concrete is very beneficial to the hydration of cementitious materials in concrete, thereby ensuring that there are more cementitious products inside the concrete. These compounds can fill the pores in the concrete matrix, thereby increasing the density of concrete. As shown in Fig. 10, especially, for the S60 concrete, because of the high volume of GGBF Slag, the secondary hydration activity of GGBF slag becomes higher, which is more conducive to the formation of C−S−H gel. These gels condense through cementation to block the pores, thus reducing defects such as large pores (>50 mm) and cracks in the concrete matrix [66,71]. However, there are some tiny pores inside the gel, mainly gel pores (<50 mm).

The literatures [55,56] classifies the pore size of concrete into four levels, namely harmless pores <20 nm, less harmful pores 20 nm−50 nm, harmful pores 50 nm−200 nm, and more harmful pores>200 nm. Fig.10(e and f) shows the pore volume classification of different GGBFS concrete and its percentage of total pore volume. After the RIM test, the proportions of harmless pores in the specimens S0, S15, S30, and S60 were 38%, 45%, 41%, and 42%, respectively. The proportions of less harmful pores were 20%, 19%, 24% and 25%. The proportion of harmful pores is 17%, 13%, 11%, and 14%. The proportions of more harmful pores are 25%, 23%, 24%, and 19%. It can be seen that as the content of GGBFS increases, the proportion of harmless pores inside the GGBFS concrete after the intrusion of iodide ions also increases, while the proportion of harmful pores decreases.

Similarly, after the test of the RCM, the proportions of gel pores in the specimens S0, S15, S30, and S60 were 40%, 45%, 46%, and 44%, respectively. The transition pores accounted for 18%, 21%, 17%, 23%. Capillary pores accounted for 15%, 12%, 14%, 13%. The proportion of macro pores is 27%, 22%, 23%, 20%. The incorporation of GGBFS improves the pore structure of GGBFS concrete very well. Comparing the S0 specimens with the GGBFS specimens, the improvement effect of GGBFS is obvious. After the chloride ion invades, the proportion of harmless pores (gel pores and transition pores) in the specimens is also increasing, and the proportion of more harmful pores (Capillary pores and macro pores) is decreasing.

The above analysis shows that the GGBFS concrete after RIM and RCM test, the incorporation of GGBFS can increase the proportion of harmless pores in the GGBFS concrete and reduce the proportion of harmful pores. The GGBFS volume is
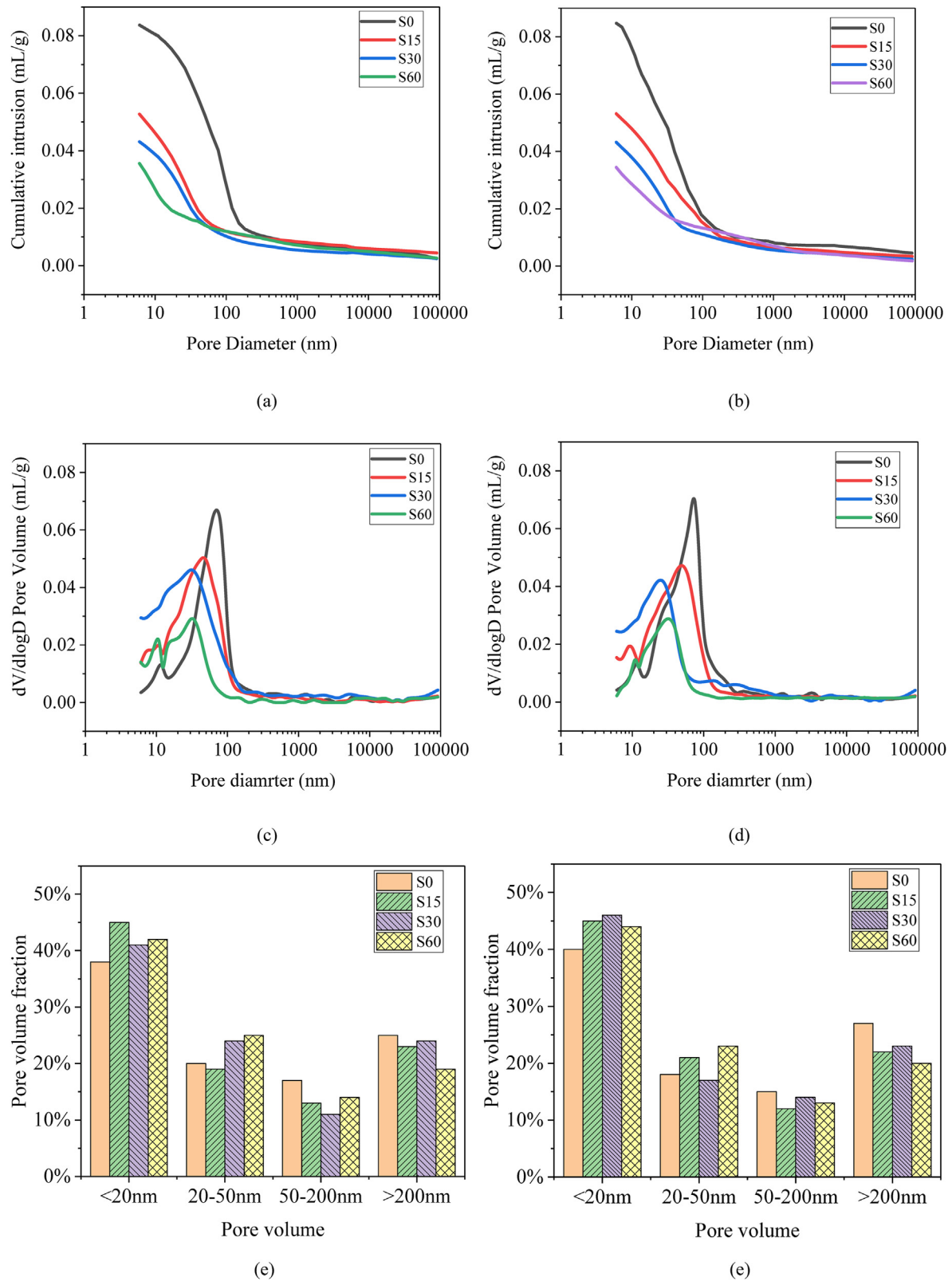
(a)

(b)

(c)

(d)

(e)

(e)

Fig. 10 — Pore structure distribution of GGBFS concrete. (a) Cumulative pore size distribution of concrete after RIM (b) Cumulative pore size distribution of concrete after RCM. (c) Differential pore size distribution of concrete after RIM (d) Differential pore size distribution of concrete after RCM. (e) Different pore size distribution of concrete after RIM (f) Different pore size distribution of concrete after RCM.

in the range of 15%−60%. As the dosage of GGBFS increases, the improvement effect on changing pores distribution and decreasing the porosity is better.

3.5. Microstructural characterization

Observing the microscopic morphology of cement paste by scanning electron microscopy (SEM) can be used to characterize the compactness of GGBFS-cement paste, the degree of hydration and morphological characteristics of GGBFS particles [57,58], etc. In this study, 150-day GGBFS concrete samples

were selected for SEM experiments to observe the microscopic morphology of the hardened GGBFS concrete after iodide and chloride ions. The results are shown in Fig. 11(a−f).

It can be seen from the micro-topography that there is no obvious difference between the GGBFS-cement slurry after the erosion of iodide ions and chloride ions. With the increase of the GGBFS content, the more irregular GGBFS particles are visible, the secondary hydration products around the GGBFS particles are also more abundant, the slurry becomes denser, and the visible pores gradually decrease. From the S30 samples, a lot of CH flaky crystals can be clearly observed, and the
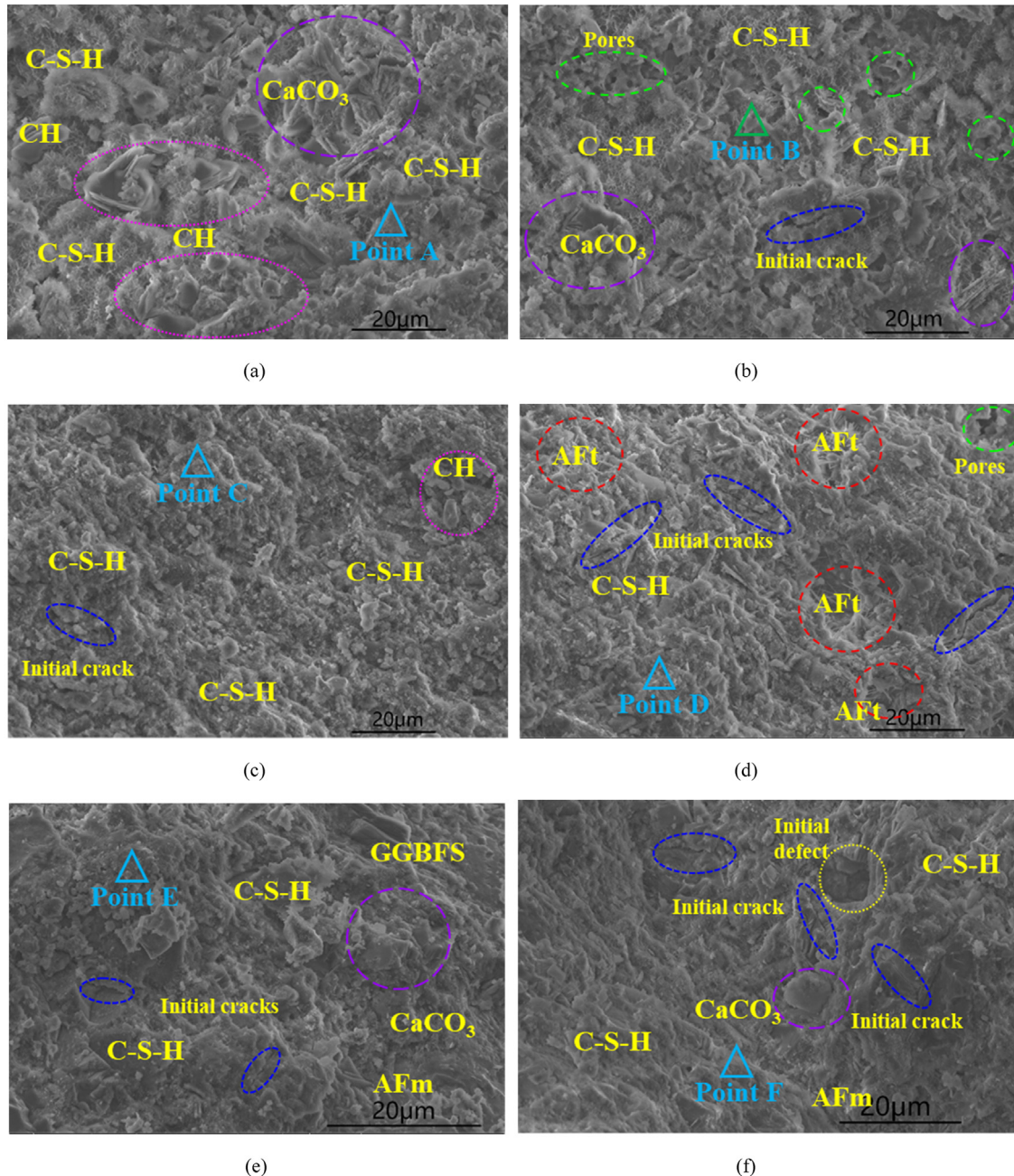

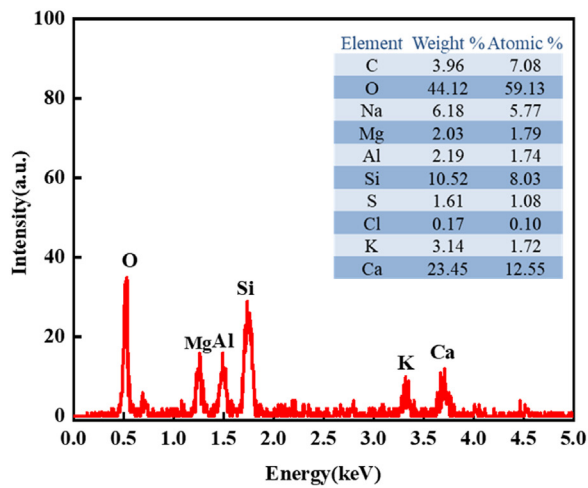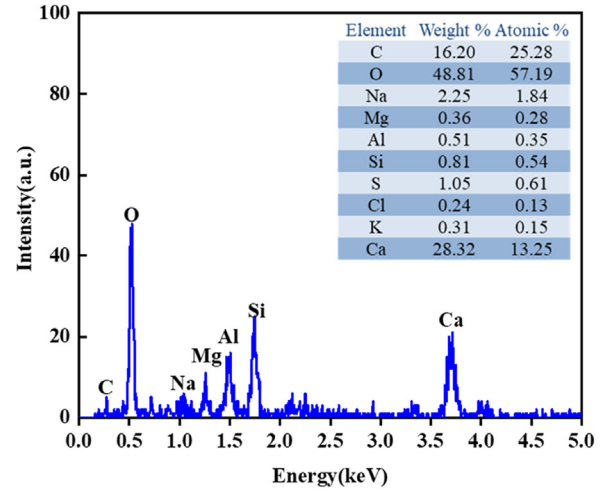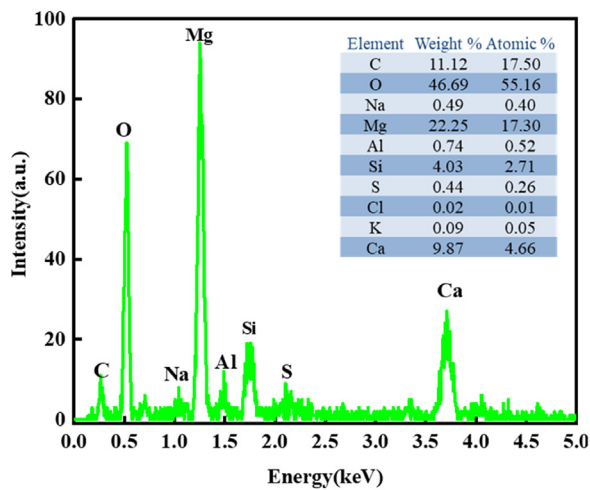Fig. 11 − Micro morphology of GGBFS concrete. (a) Microscopic morphology of S15 under chloride ion erosion (b) Microscopic morphology of S15 under erosion of iodide ion. (c) Microscopic morphology of S30 under chloride ion erosion (d) Microscopic morphology of S30 under erosion of iodide ion. (e) Microscopic morphology of S60 under chloride ion erosion (f) Microscopic morphology of S60 under erosion of iodide ion.
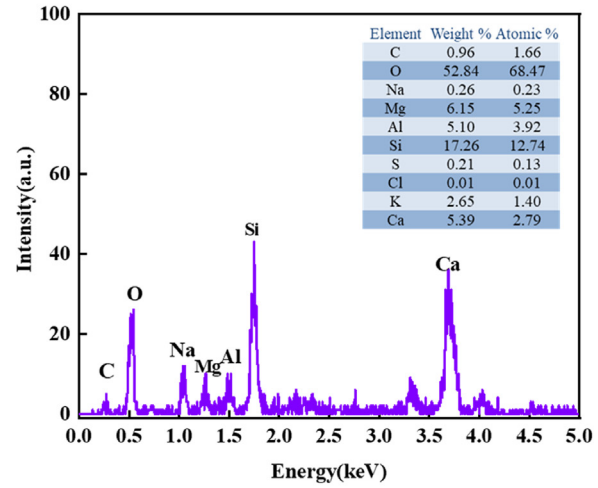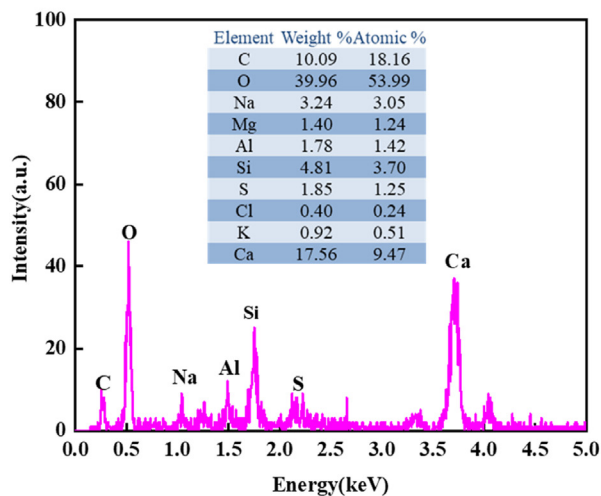
(a) Point A

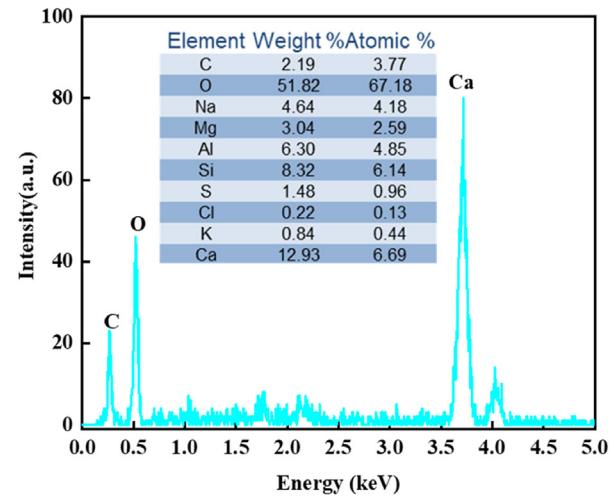| Element	Weight %	Atomic %
C	3.96	7.08
O	44.12	59.13
Na	6.18	5.77
Mg	2.03	1.79
Al	2.19	1.74
Si	10.52	8.03
S	1.61	1.08
Cl	0.17	0.10
K	3.14	1.72
Ca	23.45	12.55

(b) Point B

Element	Weight %	Atomic %
C	16.20	25.28
O	48.81	57.19
Na	2.25	1.84
Mg	0.36	0.28
Al	0.51	0.35
Si	0.81	0.54
S	1.05	0.61
Cl	0.24	0.13
K	0.31	0.15
Ca	28.32	13.25

(c) Point C

Element	Weight %	Atomic %
C	11.12	17.50
O	46.69	55.16
Na	0.49	0.40
Mg	22.25	17.30
Al	0.74	0.52
Si	4.03	2.71
S	0.44	0.26
Cl	0.02	0.01
K	0.09	0.05
Ca	9.87	4.66

(d) Point D

Element	Weight %	Atomic %
C	0.96	1.66
O	52.84	68.47
Na	0.26	0.23
Mg	6.15	5.25
Al	5.10	3.92
Si	17.26	12.74
S	0.21	0.13
Cl	0.01	0.01
K	2.65	1.40
Ca	5.39	2.79

(e) Point E

Element	Weight %	Atomic %
C	10.09	18.16
O	39.96	53.99
Na	3.24	3.05
Mg	1.40	1.24
Al	1.78	1.42
Si	4.81	3.70
S	1.85	1.25
Cl	0.40	0.24
K	0.92	0.51
Ca	17.56	9.47

(f) Point F

Element	Weight %	Atomic %
C	2.19	3.77
O	51.82	67.18
Na	4.64	4.18
Mg	3.04	2.59
Al	6.30	4.85
Si	8.32	6.14
S	1.48	0.96
Cl	0.22	0.13
K	0.84	0.44
Ca	12.93	6.69

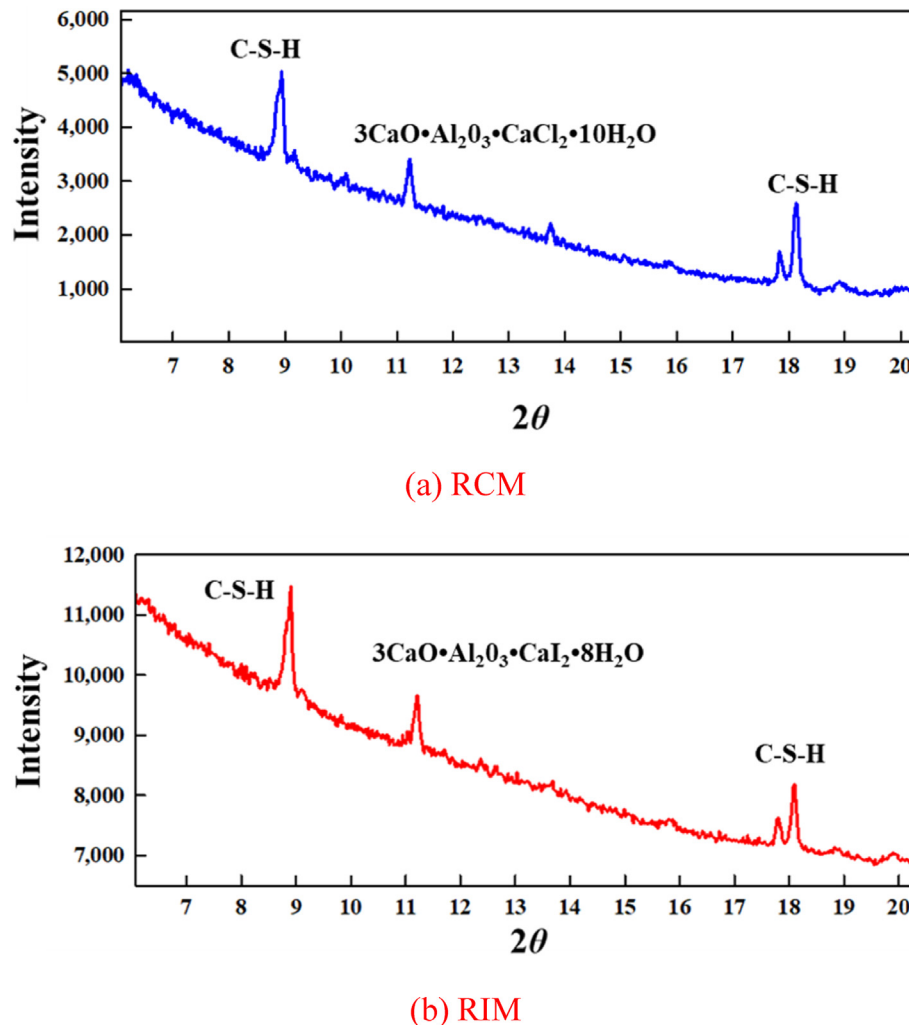Fig. 12 — EDS of GGBFS concrete.

(a) RCM

(b) RIM

Fig. 13 — XRD patterns of concrete with GGBF Slag.

fibrous C—S—H gel is abundant. When the dosage is 60%, the CH crystals in the samples are reduced, and the slurry has become very dense, which is in good agreement with the pore results measured by the MIP experiment.

In addition, in concrete containing GGBF slag, the main hydration products are C—S—H and CH. The distribution of C—S—H in concrete containing 15% GGBF slag is dense and uniform. In contrast, the hydration products of concrete containing 30% GGBF slag are complex, including C—S—H, AFt, CH and some hydration phases similar to salt impurities. Literature [59] also found that in OPC slurry containing seawater, there are more unhydrated cement particles at 63 days, and seawater may reduce the hydration rate in the later stage of OPC. In addition, there are significant differences in the surface morphology of hydration products between concrete containing 15% GGBF slag and concrete containing 60% GGBF slag. A large number of hexagonal crystals AFm are found in concrete containing 60% GGBF slag, which are the hydration products of C4AF. As for the concrete containing 60% GGBF slag, a large number of hexagonal crystals AFm are closely intertwined with C—S—H and other hydration products, making the matrix structure denser than that of concrete containing 15% GGBF slag, thereby reducing the

porosity of the concrete, which is consistent with the MIP analysis.

In order to further determine the microscopic effect of concrete resisting corrosive ion penetration under different GGBF slag content, a drawing analysis of energy spectrum elements was carried out. The element distribution diagrams of concrete containing 15% GGBF slag, concrete containing 30% GGBF slag and concrete containing 60% GGBF slag are shown in Fig. 12. Research has found that the hydration products of concrete containing 15% GGBF slag are complex. In addition to C—S—H, CH and AFt, it also contains salt impurities such as calcium carbonate and magnesium carbonate. These salt impurities caused by the abundant chloride and iodide solutions in the corrosive solution have been found to be another possible reason for the slight decrease in the compressive strength of seawater and sea sand concrete [60]. In the concrete containing 15% GGBF slag, the content of Al is high and the content of Fe is low in the AFm phase. In contrast, the AFm phase of concrete containing 60% GGBF slag appears to have a higher Fe/Al ratio. The iron in AFm mainly comes from C4AF, and the Fe/Al ratio has a great influence on the corrosion resistance of the ferrite phase including C4AF and its hydration products including AFm [61]. In addition, the

Fe/Al ratio of AFm in 60% GGBF slag concrete and 15% GGBF slag concrete are 0.78 and 1.13, respectively. Compared with concrete containing 60% GGBF slag, concrete containing 15% GGBF slag has a higher Fe/Al ratio in the AFm phase. This also further shows that corrosive ions (such as iodide or chloride ions, etc.) can accelerate the hydration of C4AF to form AFm. Studies have shown that this acceleration can increase the early mechanical strength of concrete and densify the microstructure of concrete [62]. In addition, with the increase of the GGBF slag content, the calcium and oxygen elements in the concrete gradually increase, which indicates that the calcium carbonate hydrated gradually increases. This also shows that as the GGBF slag helps to promote the hydration of concrete, the matrix of 60% GGBF slag concrete is denser. This result is consistent with the result of MIP analysis.

It can be observed from the comparison of Fig. 11 that the microscopic morphology of the internal slurry of the GGBFS concrete after the RIM and RCM tests are similar. Literature [52] found that the hydration product $3CaO \cdot Al_2O_3 \cdot CaI_2 \cdot 8H_2O$ of iodide ion in concrete mixed with GGBFS through XRD test is similar to the hydration products of chloride ion $3CaO \cdot Al_2O_3 \cdot CaCl_2 \cdot 10H_2O$ (Friedel salt). This indicates that iodide ions and chloride ions have similar effects on the micro morphology of the internal slurry of GGBFS concrete.

3.6. Hydration products analysis of concrete mixed with GGBF slag

It can be seen from Fig. 13 that after the RCM and RIM test of the concrete mixed with GGBFS, the hydration products of chloride ions and iodide ions will appear in the concrete, which are $3CaO \cdot Al2O3 \cdot CaI2 \cdot 8H2O$ and $3CaO \cdot Al2O3 \cdot CaCl2 \cdot 10H2O$. The peak value of these two compounds is about 11°, which also proves the conclusion in Section 3.2, and this is also very similar to the conclusion of the literature [52]. In addition, there are a large amount of C−S−H gel inside the concrete, with peak values of 9° and 18°, respectively. It can also be seen from the XRD pattern that the peak value of the C−S−H gel is relatively high, which also indicates that there is a large amount of C−S−H gel inside the concrete, which is also very similar to the findings of Section 3.4.

4. Conclusions

This subject systematically studied the diffusion and distribution of corrosive ions in GGBFS concrete and plain concrete, and analyzed the pore structure and micro morphology of GGBFS concrete through SEM, MIP. The conclusions are as follows.

(1) In the RIM and RCM tests, as the content of GGBFS increases, the penetration depth of iodide and chloride ions in concrete gradually decreases. As the longer the curing period is, the stronger the ion permeability resistance of GGBFS concrete is. At the same GGBFS content, the penetration depth of iodide ions in concrete is slightly greater than the diffusion depth of chloride ions.

(2) In the RIM and RCM tests, as the penetration depth increases, the concentration of free iodide and chloride ions in GGBFS concrete gradually decreases. With the greater the content of GGBFS, the smaller the free ion concentration at the same penetration depth is. The concentration of free iodide ions at the same penetration depth is slightly greater than that of free chloride ions.

(3) Iodine ions and chloride ions have similar effects on the pore structure and microscopic morphology of the hardened GGBFS concrete slurry. With the increase of GGBFS content, the cumulative pore volume and the most probable pore of GGBFS concrete gradually decrease. After iodide ions and chloride ions invade the concrete, they have similar effects on the distribution of different pores of the specimens. GGBFS can increase the proportion of transition pores and gel pores in the concrete, and decrease the proportion of macropores and capillary pores.

(4) As the content of GGBFS increases, the diffusion coefficient of iodide and chloride ions in concrete gradually decreases. Among them, the iodine ion diffusion coefficient is 1.085–1.184 times that of the chloride ion diffusion coefficient. Based on the data regression analysis method, the relationship between the GGBFS content and the corrosion ion adjustment coefficient α and β is fitted. After the iodine ion diffusion coefficient of GGBFS concrete is adjusted and transformed, the error value meets the engineering accuracy requirements and can be used as the chloride ion diffusion coefficient of GGBFS concrete. This provides some ideas and experience for the study of chloride ion diffusion in chloride-containing concrete.

Declaration of Competing Interest

The authors declare that they have no known competing financial interests or personal relationships that could have appeared to influence the work reported in this paper.

Acknowledgements

REFERENCES

[1] Al-Mattarneh H. Determination of chloride content in concrete using near and far-field microwave non-destructive methods. Corrosion Sci 2016;105:133—40.

[2] Cao C, Cheung MMS, Chan BYB. Modelling of interaction between corrosion-induced concrete cover crack and steel corrosion rate. Corrosion Sci 2013;69:97–109.

[3] Williamson J, Isgor OB. The effect of simulated concrete pore solution composition and chlorides on the electronic properties of passive films on carbon steel rebar. Corrosion Sci 2016;106:82–95.

[4] Pour-Ali S, Dehghanian C, Kosari A. Corrosion protection of the reinforcing steels in chloride-laden concrete environment through epoxy/polyaniline–camphorsulfonate nanocomposite coating. Corrosion Sci 2015;90:239–47.

[5] Andrade C. Propagation of reinforcement corrosion: principles, testing and modelling. Mater Struct 2019;52:1–26.

[6] Liu J, Qiu Q, Chen X, Wang X, Xing F, Han N, et al. Degradation of fly ash concrete under the coupled effect of carbonation and chloride aerosol ingress. Corrosion Sci 2016;112:364–72.

[7] Nace-International-Report.pdf. 2021 (n.d.), http://impact.nace.org/documents/Nace-International-Report.pdf. [Accessed 18 April 2019].

[8] Liu J, Qiu Q, Chen X, Xing F, Han N, He Y, et al. Understanding the interacted mechanism between carbonation and chloride aerosol attack in ordinary Portland cement concrete. Cement Concr Res 2017;95:217–25.

[9] Liu J, Tang K, Qiu Q, Pan D, Lei Z, Xing F. Experimental investigation on pore structure characterization of concrete exposed to water and chlorides. Materials 2014;7(9):6646–59.

[10] Song Z, Jiang L, Chu H, Xiong C, Liu R, You L. Modeling of chloride diffusion in concrete immersed in CaCl2 and NaCl solutions with account of multi-phase reactions and ionic interactions. Construct Build Mater 2014;66:1–9.

[11] Cherif R, Hamami A, Aït-Mokhtar A. Effects of leaching and chloride migration on the microstructure and pore solution of blended cement pastes during a migration test. Construct Build Mater 2020;240:117934.

[12] Li D, Li L, Wang X. Chloride diffusion model for concrete in marine environment with considering binding effect. Mar Struct 2019;66:44–51.

[13] Liu P, Yu Z, Lu Z, Chen Y, Liu X. Predictive convection zone depth of chloride in concrete under chloride environment. Cement Concr Compos 2016;72:257–67.

[14] Simčič T, Pejovnik S, De Schutter G, Bosiljkov VB. Chloride ion penetration into fly ash modified concrete during wetting–drying cycles. Construct Build Mater 2015;93:1216–23.

[15] Chia KS, Zhang M-H. Water permeability and chloride penetrability of high strength lightweight aggregate concrete. Cement Concr Res 2002;32:639–45.

[16] Liu J, Qiu Q, Xing F, Pan D. Permeation properties and pore structure of surface layer of fly ash concrete. Materials 2014;7(6):4282–96.

[17] Zhao Y, Dong J, Wu Y, Wang H, Li X, Xu Q. Steel corrosion and corrosion induced cracking in recycled aggregate concrete. Corrosion Sci 2014;85:241–50.

[18] Park B, Jang SY, Cho J-Y, Kim JY. A novel short-term immersion test to determine the chloride ion diffusion coefficient of cementitious materials. Construct Build Mater 2014;57:169–78.

[19] Ma H. Multi-scale modeling of the microstructure and transport properties of contemporary concrete (Ph.D. thesis). The Hong Kong University of Science and Technology; 2013.

[20] Liu Jun, Ou Guangfeng, Qiu Qiwen, Chen Xiaochi, Jing Hong, Xing Feng. Chloride transport and microstructure of concrete with/without fly ash under atmospheric chloride condition. Construct Build Mater 2017;146:493–501.

[21] Lay* S, Liebl S, Hilbig H, Schießl P. New method to measure the rapid chloride migration coefficient of chloride-contaminated concrete. Cement Concr Res 2004;34:421–7.

[22] Dong B, Qiu Q, Xiang J, Huang C, Sun H, Xing F, et al. Electrochemical impedance interpretation of the carbonation behavior for fly ash–slag–cement materials. Construct Build Mater 2015;93:933–42.

[23] Wang X, Huang J, Dai S, Ma B, Tan H, Jiang Q. Effect of silica fume particle dispersion and distribution on the performance of cementitious materials: a theoretical analysis of optimal sonication treatment time. Construct Build Mater 2019;212:549–60.

[24] Thomas MDA, Bremner T. Performance of lightweight aggregate concrete containing slag after 25 years in a harsh marine environment. Cement Concr Res 2012;42:358–64.

[25] Tang L, Utgenannt P. A field study of critical chloride content in reinforced concrete with blended binder. Mater Corros 2009;60:617–22.

[26] Thomas M, Scott A, Bremner T, Bilodeau A, Day D. Performance of slag concrete in marine environment. ACI Mater J 2008;105:628–34.

[27] Cabrera JG, Nwaubani SO. The microstructure and chloride ion diffusion characteristics of cements containing metakaolin and fly ash. Fly Ash, Silica Fume, Slag and Natural Pozzolans in Concrete 1998:385–400.

[28] Ganjian E, Pouya HS. The effect of Persian Gulf tidal zone exposure on durability of mixes containing silica fume and blast furnace slag. Construct Build Mater 2009;23:644–52.

[29] Fajardo G, Valdez P, Pacheco J. Corrosion of steel rebar embedded in natural pozzolan based mortars exposed to chlorides. Construct Build Mater 2009;23:768–74.

[30] Yang P, Sant G, Neithalath N. A refined, self-consistent Poisson-Nernst-Planck (PNP) model for electrically induced transport of multiple ionic species through concrete. Cement Concr Compos 2017;82:80–94.

[31] Page CL, Short NR, Holden WR. The influence of different cements on chloride-induced corrosion of reinforcing steel. Cement Concr Res 1986;16:79–86.

[32] Page CL, Vennesland O. Pore solution composition and chloride binding capacity of silica fume-cement pastes. Mater Struct 1983;16:19–25.

[33] Luo T, Wang Q, Zhuang SY. Effects of ultra-fine ground granulated blast-furnace slag on initial setting time, fluidity and rheological properties of cement pastes. Powder Technol 2019;345:54–63.

[34] Connell M. The long term performance of high slag concrete. Concrete 1998;32:30–1.

[35] Dhir RK, El-Mohr MAK, Dyer TD. Chloride binding in GGBS concrete. Cement Concr Res 1996;26:1767–73.

[36] Luo R, Cai Y, Wang C, Huang X. Study of chloride binding and diffusion in GGBS concrete. Cement Concr Res 2003;33:1–7.

[37] ASTM C150. Standard specification for Portland cement. West Conshohocken, United States: ASTM International; 2016.

[38] ASTM C33/C33M. Standard specification for concrete aggregates. West Conshohocken, PA: ASTM International; 2016.

[39] Liu Jun, Hu Lu, Tang Luping, Ren Jun. Utilisation of municipal solid waste incinerator (MSWI) fly ash with metakaolin for preparation of alkali-activated cementitious material. J Hazard Mater 2021;402:123451.

[40] NT (NORDTEST) Build 443. Concrete hardened: accelerated chloride penetration, nordtest, tekniikantie 12, FIN-02150 espoo, Finland. 1995. Available online: http://www.nordtest.info/index.php/methods/building/item/concrete-hardened-accelerated-chloride-penetration-nt-build-443.html. [Accessed 8 September 2020].

[41] GB/T50082-2009. Standard testing method of testing ordinary concrete long term performance and durability. 2009.

[42] AASHTO T260-297. Standard method of test for sampling and testing for chloride ion in concrete and concrete raw

materials. Washington, United state: American Association of State Highway and Transportation Officials; 2009.

[43] Jin Hesong, Liu Jiaying, Jiang Zhilu, Zhou Hao, Liu Jun. Influence of the rainfall intensity on the chloride ion distribution in concrete with different levels of initial water saturation. Construct Build Mater 2021;281:122561.

[44] Yoo SW, Kwon S-J. Effects of cold joint and loading conditions on chloride diffusion in concrete containing GGBFS. Construct Build Mater 2016;115:247—55.

[45] Gesoglu M, Güneyisi E, Özbay E. Properties of self-compacting concretes made with binary, ternary, and quaternary cementitious blends of fly ash, blast furnace slag, and silica fume. Construct Build Mater 2009;23:1847—54.

[46] Chia KS, Zhang MH. Water permeability and chloride penetrability of high strength lightweight aggregate concrete. Cement Concr Res 2002;32:645—59.

[47] Marsh BK, Day RL, Banner DG. Pore structure characteristics affecting the permeability of cement paste containing fly ash. Cement Concr Res 1985;15:1027—38.

[48] Güneyisi E, Özturan T, Gesoglu M. Effect of initial curing on chloride ingress and corrosion resistance characteristics of concretes made with plain and blended cements. Build Environ 2007;42:2676—3685.

[49] Guneyisi E, Gesoglu M. A study on durability properties of high-performance concretes incorporating high replacement levels of slag. Mater Struct 2008;41:479—93.

[50] Rasheeduzzafar, Al-Saadoun S, Al-Gahtani AS, et al. Effect of tricalcium aluminate content of cement on corrosion of reinforcing steel in concrete. Cement Concr Res 1990;20(5):723—38.

[51] Suryavanshi AK, Scantlebury JD, Lyon SB. The binding of chloride ions by sulphate resistant portland cement. Cement Concr Res 1995;25(3):581—92.

[52] Shen Zhong. Study on the natural iodide ion diffusion coefficient of concrete. Master's thesis. Shenzhen University; 2018 [(In Chinese)].

[53] Chang Haiyan. Study on the relationship between chloride ion behavior and microstructure in concrete mixed with mineral admixtures under a wide range of water-binder ratios. Master's thesis. Guangxi University; 2010 [(In Chinese)].

[54] Qiang Y, Shi C, Schutter GD, Katrien Audenaert, Deng Dehua. Chloride binding of cement-based materials subjected to external chloride environment — a review. Construct Build Mater 2009;23(1):1—13.

[55] Zhang M-H, Islam J. Use of nano-silica to reduce setting time and increase early strength of concretes with high volumes of fly ash or slag. Construct Build Mater 2012;29:573—80.

[56] Jiang Peng, Jiang Linhua, Zha Jie, Song Zijian. Influence of temperature history on chloride diffusion in high volume fly ash concrete. Construct Build Mater 2017;144:677—85.

[57] Hadjsadok A, Kenai S, Courard L, Anne Darimont. Microstructure and durability of mortars modified with medium active blast furnace slag. Construct Build Mater 2011;25(2):1018—25.

[58] Sajedi F, Razak HA, Mahmud HB, Payam Shafigh. Relationships between compressive strength of cement—slag mortars under air and water curing regimes. Construct Build Mater 2012;31(June 2012):188—96.

[59] Li P, Li W, Yu T, Qu F, Tam VWY. Investigation on early-age hydration, mechanical properties and microstructure of seawater sea sand cement mortar. Construct Build Mater 2020;249:118776.

[60] Younis A, Ebead U, Suraneni P, Nanni A. Fresh and hardened properties of seawater-mixed concrete. Construct Build Mater 2018;190:276—86. https://doi.org/10.1016/j.conbuildmat.2018.09.126.

[61] Zhang K, Lu Y, Rao M, Zhang W, Wang F. Understanding the role of brownmilerite on corrosion resistance. Construct Build Mater 2020;254:119262.

[62] Han Shiwen, Zhong Jing, Ding Weijian, Ou Jinping. Strength, hydration, and microstructure of seawater sea-sand concrete using high-ferrite Portland cement. Construct Build Mater 2021;295:123703.

[63] Chinese cement: common Portland cement in GB175-2007. Beijing, China: Chinese National Standard; 2007 [(In Chinese)].

[64] ASTM C989. Standard specification for slag cement for use in concrete and mortars. West Conshohocken, United States: ASTM International; 2017.

[65] Liu Jun. Permeability evaluation method of concrete based on the transport characteristics of iodide ions. Changsha, China: Central South Univ; 2013.

[66] Liu Jun, Zhang Weizhuo, Li Zhenlin, Jin Hesong, Tang Luping. Influence of deicing salt on the surface properties of concrete specimens after 20 years. Construct Build Mater 2021;295:123643.

[67] Zhang Jingxiao, Ma Yuwei, Zheng Jiazheng, Jie Hu, Jiyang Fu, Zhang Zuhua, et al. Chloride diffusion in alkali-activated fly ash/slag concretes: role of slag content, water/binder ratio, alkali content and sand-aggregate ratio. Construct Build Mater 2020;261:119940.

[68] Babaee M, Castel A. Chloride diffusivity, chloride threshold, and corrosion initiation in reinforced alkali-activated mortars: role of calcium, alkali, and silicate content. Cement Concr Res 2018;111:56—71.

[69] Hu X, Shi C, Shi Z, Zhang L. Compressive strength, pore structure and chloride transport properties of alkali-activated slag/fly ash mortars. Cement Concr Compos 2019;104:103392.

[70] Bondar D, Basheer M, Nanukuttan S. Suitability of alkali activated slag/fly ash (AA-GGBS/FA) concretes for chloride environments: characterisation based on mix design and compliance testing. Construct Build Mater 2019;216:612—21.

[71] Fan Jingchong, Zhu Hongguang, Shi Jing, Li Zonghui, Yang Sen. Influence of slag content on the bond strength, chloride penetration resistance, and interface phase evolution of concrete repaired with alkali activated slag/fly ash. Constr.Build. Mater. 2020;263:120639.